Control of mitochondrial dynamics by dPGC1 limits Yorkie-induced oncogenic growth in *Drosophila*

Wei Qi Guinevere Sew[1], Zhiquan Li[2], Lene Juel Rasmussen[2] and Héctor Herranz[1]

[1]Department of Cellular and Molecular Medicine, University of Copenhagen, 2200 Copenhagen N, Denmark

[2]Centre for Healthy Aging, Department of Cellular and Molecular Medicine, University of Copenhagen, 2200 Copenhagen N, Denmark

Correspondence: hherranz@sund.ku.dk

Key words: mitochondria; mitochondrial dynamics; *Drosophila*; Hippo pathway; cancer; cell cycle.

Abstract

Mitochondrial function and dynamics are crucial for maintaining cellular homeostasis and overall health. Disruptions in these processes can lead to various diseases, including cancer. The Hippo signaling pathway, a universal growth regulator, plays central roles in cancer through its main effector, the Yes-associated protein (YAP), known as Yorkie (Yki) in *Drosophila*. Yki upregulation drives benign tissue overgrowth in *Drosophila* imaginal discs. Our research demonstrates that the conserved metabolic regulator dPGC1 limits Yki-driven tissue hyperplasia and maintains tissue homeostasis in vivo. Yki upregulation and dPGC1 depletion lead to tumors characterized by enlarged and hyperfused mitochondria, a condition both necessary and sufficient for Yki-driven oncogenic growth. Our findings demonstrate that mitochondrial hyperfusion elevates the levels of the cell cycle regulator Cyclin E, which is crucial for tumor development. Our findings identify dPGC1 as a context-dependent tumor suppressor that coordinates mitochondrial dynamics and cell cycle regulation in response to oncogene activation. Defects in these processes are commonly found in cancer cells, highlighting major implications for cancer development in humans.

Introduction

Cancer is a multistep process that involves the accumulation of mutations affecting different cellular functions known as the hallmarks of cancer. Those include central cellular processes such cell proliferation, apoptosis, and cellular energetics. The different hallmarks, collectively, promote the transformation of normal cells into malignant entities (Hanahan, 2022; Hanahan & Weinberg, 2011). Tumors frequently undergo major changes in their metabolism, which is required to fulfil the high energetic demands of cancer cells. Mitochondria are cytoplasmic organelles playing central roles in cellular energetics. Alterations to these functions can provide plasticity and adaptability to tumor cells growing in harsh environments such as hypoxia, reduced nutrient availability, and cancer treatments (Vyas *et al*, 2016). Alterations in mitochondria hence influence different aspects related to tumor initiation and disease progression, and genetic alterations affecting mitochondria can result in an increased risk of cancer (Pavlova & Thompson, 2016; Sullivan *et al*, 2016).

Mitochondria are highly dynamics organelles. Continuous fusion and fission events are crucial to maintain mitochondrial integrity and function. Mitochondrial fission mediates the division of one mitochondrion into two mitochondria and is central for processes such as mitosis or quality control. Mitochondrial fusion is the process by which two original mitochondria merge in one. This process allows the transfer of cellular products between mitochondria and is thus crucial for proper mitochondrial function, especially under different kinds of cellular stress (Adebayo *et al*, 2021; Mishra & Chan, 2014). Besides maintaining mitochondrial integrity and function, the balance between fission and fusion is crucial for regulating the cell cycle (Antico Arciuch *et al*, 2012; Qian *et al*, 2012). The cell cycle ensures that a cell replicates and segregates its genome faithfully before it divides into two identical daughter cells. Errors in this process could lead to genomic instability, which is a cancer driver (Tubbs & Nussenzweig, 2017). Defective mitochondrial dynamics can lead to unbalanced fusion/fission that has been associated with human diseases such as cancer. Thus, mitochondrial dynamics must be tightly regulated to ensure proper cellular functions and tissue homeostasis (Archer, 2013; Dai & Jiang, 2019; Liao *et al*, 2024; Picard *et al*, 2013; Senft & Ronai, 2016; Yu *et al*, 2023).

The Peroxisome Proliferator Activated Receptor Gamma Co-activator-1 (PGC1) family of transcriptional regulators plays central roles controlling mitochondrial biogenesis and function. In mammals, it includes PGC1α, PGC1β, and PGC1-related coactivator (PRC) (Scarpulla, 2011;

69 Villena, 2015). These family members share structural and functional similarities. Among them,
70 PGC1α is particularly significant in cancer, where it influences mitochondrial dynamics, metabolic
71 reprogramming, and tumor progression. In contrast, PGC1β and PRC are primarily involved in
72 cellular metabolism and energy homeostasis, with less pronounced roles in cancer. This distinction
73 underscores the unique and critical role of PGC1α in oncogenesis (Qian *et al*, 2024). PGC1α levels
74 can be either upregulated or downregulated in different cancer types, highlighting its dual role as a
75 tumor suppressor and an oncogene, depending on the context (Bhalla *et al*, 2011; Girnun, 2012; Jones
76 *et al*, 2012; Tan *et al*, 2016; Torrano *et al*, 2016; Wang *et al*, 2024). Therefore, understanding the
77 specific functions of PGC1α in different contexts will help to identify tumor-specific vulnerabilities
78 that can be targeted in clinical treatments. *Drosophila* is emerging as a valuable *in vivo* model to
79 study various aspects of cancer (Gonzalez, 2013). Notably, *Drosophila* possesses a sole PGC1
80 orthologue (dPGC1), that has also been involved in the regulation of energy metabolism and
81 mitochondrial function (Gershman *et al*, 2007; Mukherjee *et al*, 2014). The functional homology
82 between dPGC1 and mammalian PGC1 members facilitates the study of PGC1 functions in
83 *Drosophila* without the complications of redundancy.

84 The Hippo signaling pathway is a conserved regulator for normal and oncogenic growth. The central
85 elements of this pathway comprise a regulatory kinase cascade that, when active, limits tissue growth
86 by phosphorylating and inhibiting the activity of Transcriptional co-Activator with PDZ-binding
87 motif (TAZ) and Yes-associated protein (YAP), Yorkie (Yki) in *Drosophila* (Zheng & Pan, 2019).
88 Deregulation in the activity of the Hippo pathway affects tumor development and has been associated
89 with traits of oncogenesis such as cell proliferation and survival, cancer metabolism, invasion, and
90 metastasis (Barron & Kagey, 2014; Moon *et al*, 2018). Consistently with their growth regulatory
91 roles, YAP and TAZ are frequently amplified, while upstream elements in the pathway are mutated
92 in different cancer types (Calses *et al*, 2019).

93 In this study, we find that although depletion of the transcriptional coactivator *dPGC1* does not affect
94 the normal development of *Drosophila* wing imaginal discs, it drives tumor growth and cellular
95 transformation in imaginal discs over-expressing *Yki*. These results provide *in vivo* evidence
96 supporting that dPGC1 is a context dependent tumor suppressor. We show dPGC1 limits
97 tumorigenesis and maintains tissue homeostasis by regulating mitochondrial dynamics. We show that
98 tumors driven by Yki upregulation and dPGC1 depletion exhibit large mitochondria. We find that
99 hyperfused mitochondria promote oncogenesis by upregulating the oncogene Cyclin E, which

100 induces tumor growth and causes DNA damage, two well-known hallmarks of cancer. This study
101 connects aberrant mitochondrial dynamics with defective cell cycle regulation and DNA damage, in
102 oncogenic processes *in vivo*.
103

104 # Results

105 **Normal Wing Development is not Affected by *dPGC1* Depletion**

106 The systemic functions of dPGC1 have been extensively studied and has been shown to control
107 central physiological processes such as early development, tissue homeostasis, obesity, and aging
108 (Chen *et al*, 2012; Diop *et al*, 2015; George & Jacobs, 2019; Mukherjee *et al.*, 2014; Mukherjee &
109 Duttaroy, 2013; Rera *et al*, 2011; Rogers & Rogina, 2014). However, the roles played by this
110 transcriptional regulator in proliferating tissues such as developing organs or tumors have not been
111 elucidated yet. Here, we have used the wing imaginal disc of *Drosophila* to study the functions of
112 dPGC1 in proliferating epithelia. The wing disc of *Drosophila* is composed of a proliferative
113 epithelium that, after metamorphosis, gives rise to the wing and thorax of the adult fly. This organ is
114 a common *in vivo* model to study development, growth control, and tumor formation (Herranz *et al*,
115 2016).

116 The Gal4-UAS binary system allows to manipulate gene activity in a time- and tissue-specific manner
117 (Brand & Perrimon, 1993). We used this genetic tool to differentiate the systemic functions of dPGC1
118 from its cell autonomous role in the proliferating imaginal epithelia. The MS1096-Gal4 line is
119 expressed in the wing disc (Fig 1A). It allows us to manipulate gene activity during the development
120 of this organ and analyze the resulting phenotypic outcomes in the adult wing. Consistent with
121 previous observations (Tiefenböck *et al*, 2010), depletion of *dPGC1* by the expression of UAS-RNAi
122 transgenes under the control of MS1096-Gal4 did not have a major impact on adult wing size and
123 shape (Fig 1B, C). We obtained comparable results using an independent UAS-dPGC1-shRNA line
124 (Fig S1). The efficiency of the transgenes used to deplete *dPGC1* is shown in Fig S1. These
125 observations are consistent with studies in mice showing that PGC1α and PGC1β are nonessential
126 for normal development (Lelliott *et al*, 2006; Leone *et al*, 2005; Lin *et al*, 2004; Sonoda *et al*, 2007;
127 Vianna *et al*, 2006). As observed in wings downregulating *dPGC1*, overexpression of *dPGC1* did not
128 affect wing size (Fig 1B, C; Fig S1). These results indicate that changes in dPGC1 levels do not have
129 a major impact on the normal growth and development of the *Drosophila* wing.

130

131 **dPGC1 Dampens Yki-Induced Tissue Over-Growth**

132 Transcriptional coregulators such as the members of the PGC1 family have been proposed to fine-
133 tune and optimize mitochondrial function to adapt cell metabolism in response to environmental cues
134 (Mouchiroud *et al*, 2014; Scarpulla, 2011). A central element mediating cellular responses to
135 extracellular stimulus is the Hippo signaling pathway. The activity of this signaling module is
136 controlled by extracellular cues such as mechanical tension, hypoxia, or nutritional conditions (Koo
137 & Guan, 2018; Varelas, 2014; Yu *et al*, 2015). The protooncogene Yki is the main effector of the
138 Hippo pathway in *Drosophila*. Yki drives growth by controlling cell cycle progression and inhibiting
139 apoptosis (Gerlach *et al*, 2018; Gerlach *et al*, 2019; Huang *et al*, 2005; Nolo *et al*, 2006; Thompson
140 & Cohen, 2006). Additionally, Yki modulates mitochondrial structure and function, which is also a
141 central aspect in the growth-promoting role of this protooncogene (Nagaraj *et al*, 2012).

142 The results showing that Yki induces mitochondrial changes to support tissue growth, together with
143 the notion that transcriptional regulators could refine these kind of processes (Mouchiroud *et al.*,
144 2014; Nagaraj *et al.*, 2012), led us to study whether dPGC1 influences the response to Yki
145 upregulation. To evaluate this, we analyzed the consequences of depleting *dPGC1* in discs
146 overexpressing *Yki*. For this analysis, we used the apterous-Gal4 (ap-Gal4) driver, which is expressed
147 in the dorsal compartment of the wing disc (Fig 2A). The use of this Gal4 driver allows to manipulate
148 gene activity in the dorsal cells of the wing disc and use the otherwise normal ventral compartment
149 as an internal control. As shown in previous analyses, expression of *Yki* in the wing imaginal disc led
150 to a robust increase in tissue size (Fig 2A, C, E) (Huang *et al.*, 2005). Although *dPGC1*
151 downregulation did not affect normal wing disc growth (Fig 2A, B, E), depletion of *dPGC1* in a
152 context of *Yki* upregulation enhanced the Yki-induced growth response (Fig 2A-E). These results
153 indicate that, although dispensable for normal wing development, dPGC1 is required to limit Yki-
154 driven tissue overgrowth.

155

156 **Oncogenic Features in Tumors Driven by *Yki* Overexpression and *dPGC1* Depletion**

157 To gain better insights about the tumor suppressive roles of dPGC1, we investigated whether other
158 oncogenic properties were present in those tumorous discs, in addition to the observed increase in

159 tissue size. Malignant fly tumors express the secreted matrix metalloproteinase 1 (Mmp1), which
160 contributes to cell migration and subsequent invasion by mediating the degradation of the basement
161 membrane (Beaucher *et al*, 2007; Uhlirova & Bohmann, 2006). While we did not detect Mmp1
162 expression in control discs (ap>GFP), Mmp1 was observed in discrete patches of cells in discs over-
163 expressing *Yki* (Fig 2F, G). Notably, discs coexpressing *Yki* and *dPGC1-RNAi* displayed a robust
164 increase in Mmp1 (Fig 2G, H). Mmp1 is a target gene of the c-Jun N-terminal kinase (JNK) pathway.
165 This signaling cascade is activated by internal and external stressors and control different biological
166 processes such as proliferation, apoptosis, and cell migration (La Marca & Richardson, 2020; Pinal
167 *et al*, 2019). JNK is an oncogenic partner of pro-tumorigenic elements such as RasV12 and Yki (Igaki
168 *et al*, 2006; Uhlirova & Bohmann, 2006). In these contexts, JNK induces the accumulation of F-actin,
169 which is observed in cells undergoing malignant transformation (Enomoto *et al*, 2015; Fernandez *et*
170 *al*, 2011; Fernandez *et al*, 2014; George & Jacobs, 2019; Khoo *et al*, 2013; Uhlirova & Bohmann,
171 2006). In good agreement with those results, we detected an increase in F-actin levels in Yki +
172 dPGC1-RNAi tumorous discs. This correlated with the presence of JNK-target gene Mmp1 (Fig 2G,
173 H). Similar results were obtained by an independent UAS-dPGC1-shRNA line (Fig S2).

174 In sum, our results show that *dPGC1* knockdown enhances Yki-induced overgrowth, leading to the
175 formation of tumorous discs that exhibit markers of malignancy. Although *dPGC1* depletion does not
176 have a major impact on normal growth, it is required to maintain controlled growth and tissue
177 homeostasis in a context of Yki upregulation.

178

179 **Aberrant Mitochondrial Dynamics in Tumorous Discs Driven by Yki Over-expression and**
180 **dPGC1 Downregulation**

181 PGC1 proteins regulate the expression of genes involved in mitochondrial biogenesis and function
182 (Villena, 2015). Previous analyses have shown that Yki modulates mitochondrial dynamics to support
183 tissue growth (Nagaraj *et al.*, 2012). We analyzed whether *dPGC1* downregulation in a context of
184 Yki activation affected the expression of genes involved in these processes. By using quantitative
185 PCR (qPCR), we compared the mRNA levels of genes involved in different aspects of mitochondrial
186 dynamics such as mitochondrial biogenesis, mitochondrial fusion and fission, mitophagy, and
187 mitochondrial transport (Archer, 2013). Among genes controlling mitochondrial biogenesis, we
188 quantified the expression of *estrogen-related receptor* (*dERR*), *Ets at 97D* (*Ets97D*), and *erect wing*

189 (*ewg*) (Baltzer et al, 2009; Chen et al, 2008; Misra et al, *2017*; Rai et al, 2014; Takata et al, 2001).
190 We also assessed the expression of the genes *Mitofusin* (*dMfn*, also known as *Marf*) and *Optic Atrophy*
191 *1* (*Opa1*), which control fusion between outer and inner membranes, respectively; and *Drp1* that
192 mediates mitochondrial fission (Deng et al, 2008). Additionally, we quantified the expression of
193 genes involved in mitophagy including *PTEN-induced putative kinase 1* (*Pink1*), *parkin* (*park*), and
194 *Autophagy-related 7* (*Atg7*) (Narendra et al, 2010; Vincow et al, 2013). Finally, we measured the
195 levels of genes involved in mitochondrial transport such as *milton* (*milt*) and *mitochondrial Rho*
196 (*miro*) (Guo et al, 2005; Stowers et al, 2002). We analyzed four independent biological replicates
197 where we compared mRNA levels between Yki-upregulating discs (control) and Yki + dPGC1-RNAi
198 tumorous discs (experimental condition). We found that discs coexpressing Yki and dPGC1-RNAi
199 showed a significant increase in the expression of *dMfn* and *Opa1*, GTPases promoting mitochondrial
200 fusion (Fig 3A). Interestingly, *milt* and *miro* were also upregulated in Yki + dPGC1-RNAi tumorous
201 discs (Fig 3A). Although miro and milt play central roles in mitochondrial axonal transport, previous
202 reports have suggested that they can also promote mitochondrial fusion (Ding *et al*, 2016; Liu &
203 Hajnoczky, 2009; Panchal & Tiwari, 2020; Tang, 2015). For instance, *miro* overexpression in
204 *Drosophila* models of Alzheimer's disease have been reported to cause an increased in mitochondrial
205 average length (Panchal & Tiwari, 2020).

206 The functions of *dMfn, OPA1, milt*, and *miro* (genes upregulated in Yki + dPGC1-RNAi tumorous
207 discs) have been studied and determined in different models (Archer, 2013; Chan, 2020; Lee & Lu,
208 2014; Zorzano *et al*, 2010). However, the effects of altering the expression of those elements in
209 mitochondria of the wing imaginal disc have not been established yet. This led us to analyze the
210 consequences of manipulating those genes during the development of the wing imaginal disc. To
211 visualize mitochondria, we drove the expression of mitochondrial-targeted GFP (Mito-GFP). This
212 transgene contains mitochondrial localization sequences that target GFP to the mitochondria (Rizzuto
213 *et al*, 1995). We performed this analysis in the peripodial membrane of the wing imaginal disc. The
214 imaginal discs have a sac-like anatomy with two opposing epithelial surfaces composed by a
215 columnar epithelium on one side, known as main epithelium, and a flat squamous epithelium on the
216 other side, known as peripodial membrane (Gibson & Schubiger, 2001). The main epithelium is
217 formed by small cells densely packed. Consequently, mitochondria were difficult to visualize in that
218 epithelium (Fig 3B). In contrast, the peripodial membrane contains flat cells with a large cytoplasm.
219 Mitochondria appeared as clear and well-defined structures in the peripodial membrane (Fig 3C). The

220 peripodial membrane hence provides an amenable *in vivo* context to analyze changes in mitochondrial
221 morphology.

222 The Grunge-Gal4 (Gug-Gal4) driver can be used to drive transgene expression in peripodial
223 membrane cells (Gibson *et al*, 2002). We used this driver to visualize potential mitochondrial changes
224 when the genes deregulated in the Yki + dPGC1-RNAi context were experimentally manipulated.
225 dMfn and Opa1 are central factors promoting mitochondrial fusion. To confirm that this axis has a
226 similar function in the proliferating wing primordia, we expressed a UAS-dMfn transgene under the
227 control of Gug-Gal4. We observed that *dMfn* upregulation led to a connected mitochondrial network
228 indicative of an increase in fusion (Fig 3D; quantified in Fig S3). Reciprocally, depletion of *dMfn* in
229 those cells led to fragmented mitochondria (Fig 3E; quantified in Fig S3). Miro and milt form part of
230 a complex controlling mitochondrial transport, but recent studies involved them in fusion/fission
231 dynamics (Ding *et al.*, 2016; Liu & Hajnoczky, 2009; Panchal & Tiwari, 2020; Tang, 2015). In
232 agreement with the latter, overexpression of *miro* led to increased fusion and *miro* depletion resulted
233 in fragmented mitochondria in the peripodial epithelium (Fig 3F, G; quantified in Fig S3). Together,
234 these results show that dMfn/Opa1 and miro/milt promote mitochondrial fusion in the wing imaginal
235 disc.

236 Mitochondrial morphology and function are controlled by a dynamic balance between fusion and
237 fission. Changes in the activity of factors controlling those processes can lead to an imbalance in
238 mitochondrial dynamics affecting mitochondria function and cellular homeostasis (Adebayo *et al.*,
239 2021). The changes in gene expression in tumors driven by *Yki* expression and *dPGC1* depletion (Fig
240 3A) should favor an increase in mitochondrial fusion. We used electron microscopy to visualize and
241 evaluate mitochondrial size. We observed that mitochondria in Yki + dPGC1-RNAi tumorous discs
242 were larger in size as compared to mitochondria present in *Yki*-expressing discs (Fig 3H-K). These
243 observations suggest that, consistently with an upregulation in the expression of *dMfn, OPA1*, *milt*,
244 and *miro,* depletion of *dPGC1* in a context of *Yki* overexpression results in hyperfused mitochondria.

245

246 **Increased Mitochondrial Fusion Drives Tumor Formation in the Wing Disc**

247 Previous observations showed that Yki induces the expression of genes involved in mitochondrial
248 fusion, which is central for the growth-promoting role of this protooncogene (Nagaraj *et al.*, 2012).

249 Here, we have shown that *dPGC1* depletion enhances Yki-induced tissue growth and the resulting
250 tumorous discs present larger mitochondria (Fig 3). Those results, collectively, led us to speculate
251 that increased fusion could contribute to tumor formation when Yki was upregulated and *dPGC1*
252 knocked down. We reasoned that, if increased in fusion contributes to tumor formation,
253 downregulating the genes promoting fusion should limit tumor growth. We performed functional
254 analyses to test our hypothesis and observed that expression of UAS-RNAi transgenes targeting *dMfn*
255 or *Opa1* in Yki + dPGC1-RNAi tumors caused a reduction in growth as compared to Yki + dPGC1-
256 RNAi discs (Fig 4A-D, G). This suggests that mitochondrial fusion supports tissue growth in Yki +
257 dPGC1-RNAi tumors. Next, we asked whether increased fusion was sufficient to drive tumorigenesis
258 in concert with the protooncogene Yki. We found that coexpression of *Yki* and *dMfn* or *Opa1* resulted
259 in increased disc size (Fig 4A, E, F, G), suggesting that an increase in mitochondrial fusion is
260 sufficient to enhance Yki-driven tissue over-growth. Notably, those tumors upregulated markers of
261 malignancy and presented epithelial disorganization as revealed by Mmp1 and F-acting labeling,
262 respectively (Fig 4H, I). Knockdown or upregulation of those factors in otherwise normal discs led
263 to minor defects in tissue size, far in magnitude to the effect they had in a tumor context (Fig S4).
264 These results show that 1) an increase in mitochondrial fusion contributes to oncogenic cooperation
265 between Yki and dPGC1 knockdown, and 2) increase in mitochondrial fusion is sufficient to
266 synergize with Yki in tumorigenesis.

267

268 **Upregulation of Cyclin E in Tumors Caused by *Yki* upregulation and *dPGC1* Depletion**

269 Next, we studied the mechanisms by which increased mitochondrial fusion promote tumorigenesis.
270 Mounting evidence is establishing a connection between mitochondrial dynamics and the cell cycle
271 (Ma *et al*, 2020). The cell cycle must be tightly regulated to ensure that proliferating cells transmit an
272 intact copy of their genome to the progeny. Defects in cell cycle regulation can result in genomic
273 instability and the accumulation of mutations, which is a central hallmark of cancer (Hanahan, 2022;
274 Hanahan & Weinberg, 2011). Central regulators of the cell cycle are cyclin-dependent kinases
275 (CDKs) and their regulator partners, cyclins, which control CDK activity and cell cycle progression
276 (Besson *et al*, 2008; Satyanarayana & Kaldis, 2009). In addition to CDKs and cyclins, mitochondria
277 are emerging as important regulators of the cell cycle, and mitochondrial dynamics influence cell
278 cycle progression and hence the maintenance of genomic stability (Horbay & Bilyy, 2016; Lopez-
279 Mejia & Fajas, 2015; Mandal *et al*, 2005; Owusu-Ansah *et al*, 2008). Previous studies performed in

280 mammalian cells (*in vitro*) and in *Drosophila* (*in vivo*), have shown that cells with highly fused
281 mitochondria present an elevation in the levels of the oncogene Cyclin E (Finkel & Hwang, 2009;
282 Mitra, 2013; Mitra *et al*, 2012; Mitra *et al*, 2009; Qian *et al.*, 2012). Cyclin E levels peak during G1-
283 S transition activating CDK2 and inducing entry in S phase (Siu *et al*, 2012). Abnormal Cyclin E
284 levels can lead to premature entry into S phase and replicative stress, which is a central factor leading
285 to genomic instability in cancer (Gaillard *et al*, 2015; Molano-Fernandez *et al*, 2022; Saxena & Zou,
286 2022). We have shown that *dPGC1* depletion in epithelial cells with increased Yki signaling results
287 in mitochondrial hyper-fusion and, consequently, tumor formation. Those observations led us to
288 investigate whether Yki + dPGC1-RNAi tumors showed abnormal Cyclin E levels. Yki upregulation
289 on its own resulted in an increase in Cyclin E mRNA and protein levels, as compared to control discs
290 (Fig 5A, B). This is consistent with previous reports showing that Cyclin E is a Yki target gene (Shu
291 & Deng, 2017; Tapon *et al*, 2002). Notably, depletion of *dPGC1* in that context led to a further
292 increase in Cyclin E protein levels (Fig 5A). Interestingly, the increase in Cyclin E protein was not
293 accompanied by an upregulation in *cyclin E* mRNA (Fig 5B) suggesting that Cyclin E protein
294 upregulation was not due to an increase in *cyclin E* transcription. Consistently, previous reports
295 linking mitochondrial activity with Cyclin E control suggested that this regulation occurred post-
296 transcriptionally (Mandal *et al.*, 2005; Owusu-Ansah *et al.*, 2008). Together, these results suggest
297 that the increase of Cyclin E in Yki + dPGC1-RNAi tumors cannot be explained by changes in gene
298 expression and, instead, should be a consequence of an increase in protein translation, stability, or
299 both.

300 Aberrant Cyclin E levels can lead to replicative stress and DNA damage in human cells and
301 *Drosophila* (Ekholm-Reed *et al*, 2004; Molano-Fernandez *et al.*, 2022; Spruck *et al*, 1999). In
302 response to DNA damage, checkpoint proteins phosphorylate the histone H2AX (H2Av in
303 *Drosophila*) to mark the sites with damage (Blackford & Jackson, 2017; Fernandez-Capetillo *et al*,
304 2003). Antibodies recognizing the phosphorylated H2Av (pH2Av) can serve to detect DNA damage.
305 As expected, Yki overexpression led to an increase in pH2Av-positive foci (Fig 5 C, D, G). Notably,
306 this effect was enhanced when *dPGC1* was knocked down (Fic 5D, E, G), which is consistent with
307 an increase in Cyclin E. These observations revealed that *dPGC1* depletion in discs activating the
308 Yki protooncogene leads to an increase in Cyclin E levels and DNA damage. Oncogene-induced
309 DNA damage is a mutagenic source in cancer and DNA damage can promote tumorigenesis in
310 *Drosophila* (Dekanty *et al*, 2015; Gerlach & Herranz, 2020; Halazonetis *et al*, 2008). We then
311 analyzed whether Cyclin E upregulation contributed to the formation of Yki + dPGC1-RNAi tumors.

312 To study that, we removed one copy of *cyclin E* in Yki + dPGC1-RNAi tumors and analyzed if tumor
313 growth was affected. We observed that, while *cyclin E* heterozygous discs do not show growth defects
314 in otherwise normal discs (Fig 5H, I, N), reduction of Cyclin E in discs expressing Yki and depleting
315 *dPGC1* led to a dramatic reduction in tumor size (Fig 5J, L, M, N). This suggests that Cyclin E
316 upregulation is a central factor driving tumorigenesis in Yki + dPGC1-RNAi tumors. Next, we asked
317 whether Cyclin E upregulation was sufficient to enhance Yki-driven growth. The Cyclin E-dependent
318 kinase inhibitor p21/dacapo (dap) represses Cyclin E/CDK2. Consequently, reduced dap leads to an
319 increase in Cyclin E/CDK2 activity (de Nooij *et al*, 1996; Lane *et al*, 1996). We observed that *dap*
320 depletion was sufficient to enhance Yki-driven tumor growth (Fig 5 J, K, N). Interestingly, as
321 observed in the Yki + dPGC1-RNAi context, Yki + dap-RNAi tumors exhibited an increase in DNA
322 damage (Fig 5D-G). In sum, these results reveal that that *dPGC1* downregulation in a context of Yki
323 activation results in an increase in Cyclin E, the accumulation of DNA damage, and increased tumor
324 growth.

325

326 **Discussion**

327 The results presented here reveal that dPGC1 modulates the response to Yki upregulation in the wing
328 imaginal disc of *Drosophila*. Evidence supporting this includes functional analyses showing that
329 dPGC1 depletion leads to an enhanced growth response to Yki upregulation *in vivo.* Contrasting to
330 that, *dPGC1* depletion (or upregulation) in normal proliferating cells during wing development does
331 not result in overt phenotypes indicating that dPGC1 is mostly dispensable during the normal
332 development of this organ. Similar results emerged from analyses in mice demonstrating that PGC1α
333 is nonessential for normal mouse development (Leone *et al.*, 2005). Notably, PGC1α knock out mice
334 present various defects under stress, suggesting that PGC1α is an important factor in response to
335 stress (Arany *et al*, 2005; Lin *et al.*, 2004). A recent study by the Halder group has provided new
336 evidence that suggests that the Yki/YAP transcriptional input is not essential for normal growth. This
337 work shows that hyperactivation of Yki/YAP promotes ectopic tissue overgrowth through the
338 induction of an aberrant genetic program (Kowalczyk *et al*, 2022). We show that dPGC1 limits Yki
339 hyperactivation-induced tissue growth and is essential to maintain tissue homeostasis in that context.
340 These results provide evidence suggesting that dPGC1 plays central roles in response to stress driven
341 by an aberrant genetic program.

342 Our results find that dPGC1 limits tissue growth in a context of Yki overexpression. This contrasts
343 with previous analyses showing that dPGC1 has a growth-promoting role downstream of insulin
344 signaling in the *Drosophila* fat body, an organ functionally similar to the mammalian liver
345 (Tiefenböck *et al.*, 2010). Together, these results reveal a context-depended growth regulatory
346 function of this transcriptional regulator. Previous studies presented similar context-dependency in
347 the roles of these transcriptional regulators. For instance, PGC1α expression is reduced in prostate,
348 colon, breast, and ovary cancer, suggesting it suppresses cancer (Feilchenfeldt *et al*, 2004; Torrano
349 *et al.*, 2016; Watkins *et al*, 2004; Zhang *et al*, 2007). Other studies report the opposite behavior and
350 show that PGC1α can, in some contexts, promote tumorigenesis and metastasis hence acting as an
351 oncogenic factor (Bhalla *et al.*, 2011; LeBleu *et al*, 2014). Our observations, combined with these
352 results, highlight that the pro- or antitumorigenic functions of these transcriptional regulators depend
353 on the cellular context. This underscores the importance of identifying the specific conditions under
354 which they exhibit either role.

355 Yki drives tissue overgrowth by controlling gene expression. Yki, by interacting with the TEAD
356 transcription factor Scalloped (Sd), binds regulatory sequences and induce the expression of growth-
357 promoting genes including the cell cycle regulator Cyclin E and genes controlling mitochondrial
358 fusion such as dMfn and Opa1 (Bandura & Edgar, 2008; Nagaraj *et al.*, 2012; Shu & Deng, 2017;
359 Tapon *et al.*, 2002). Our results show that a major consequence of *dPGC1* depletion when Yki is
360 hyperactivated is the upregulation of various genes promoting mitochondrial fusion, which ultimately
361 results in larger mitochondria and tumorigenesis. We find that *dPGC1* depletion in otherwise normal
362 discs does not affect the expression of genes controlling fusion/fission mechanisms (Fig S4). This
363 insinuates that dPGC1 does not control the expression of those genes during the normal growth of
364 the wing imaginal disc. Instead, our data suggest that dPGC1 dampens the ability of Yki to induce
365 the expression of genes mediating mitochondrial fusion. Additional experiments will be required to
366 determine the specific molecular mechanisms underlying this function.

367 Unbalanced fusion/fission dynamics affect mitochondrial function and have central consequences
368 disrupting cellular homeostasis. Those defects have major pathological implications and have been
369 associated with human diseases including cardiovascular disorders, neurogenerative diseases, and
370 cancer (Archer, 2013; Dai & Jiang, 2019; Liao *et al.*, 2024; Picard *et al.*, 2013; Senft & Ronai, 2016).
371 How defects in mitochondrial dynamics influence tumor cells appear to depend on the cellular
372 context. The results presented here indicate that increased fusion is required to support tumor

373 proliferation. These observations agree with a previous analysis in mouse fibroblasts. This study
374 shows that fibroblasts transformed by the oncogene Ras present fused mitochondria, and cell
375 proliferation in those cells is sensitive to Mfn2 levels (Yao *et al*, 2019). A similar phenomenon has
376 been reported in *Drosophila* neuroblasts, the neural stem cells of the developing fly brain, in which
377 downregulation of dMfn and Opa1 causes defects in cell proliferation (Dubal *et al*, 2022). Similarly,
378 depletion of genes controlling fusion and fission events in *Drosophila* germ line stem cells leads to
379 stem cell loss and reduced fecundity (Garcez *et al*, 2020). Together with our work, those reports
380 provide evidence linking increased fusion and cell proliferation, which are central factors affecting
381 tumor initiation and disease progression.

382 Mitochondrial dynamics and the cell cycle are intimately coordinated. Changes in mitochondrial
383 dynamics influence cell cycle progression and vice versa (Lopez-Mejia & Fajas, 2015; Mandal *et al.*,
384 2005; Mitra, 2013; Mitra *et al.*, 2009; Owusu-Ansah *et al.*, 2008). Mitochondrial fusion has been
385 shown to stabilize and increase Cyclin E favoring G1-S progression in the cell cycle (Finkel &
386 Hwang, 2009; Mitra, 2013). Our results show that the ultimate consequence of *dPGC1* depletion in
387 the Yki-upregulation context is an increase in Cyclin E. This correlates with an increase in DNA
388 damage, which is a source of genomic instability typically present in tumors (Tubbs & Nussenzweig,
389 2017). We provide experimental evidence demonstrating that increased Cyclin E is crucial for tumor
390 growth and is a central oncogenic element in tumors driven by Yki upregulation and *dPGC1*
391 knockdown. In sum, our results find that *dPGC1* deregulation in cells with oncogenic activation leads
392 to aberrant mitochondrial dynamics and DNA damage, which are factors that contribute to known
393 hallmarks of cancer such as cancer metabolism and genomic instability.

394 ## Materials and Methods

395 ***Drosophila* strains**

396 The following stocks used in this paper were obtained from Bloomington *Drosophila* Stock Centre:
397 *Gug-Gal4* (BDSC 6773), Mito-GFP (BDSC 8443), yw (BDSC1495), *UAS-lacZ* (BDSC3956), *UAS-*
398 *dPGC1*^{RNAi} (BDSC 33914), *UAS-dPGC1* (BDSC 20009), *UAS-dMfn* (BDSC 67157), *UAS-dMfn*^{RNAi}
399 (BDSC 55189), *UAS-Opa1* (BDSC 20054), *UAS-Opa1*^{RNAi} (BDSC 32358), *UAS-miro* (BDSC 51646)
400 and *UAS-dap*^{RNAi} (BDSC 64026). *UAS-dPGC1*^{shRNA} (v330271) and *miro*^{RNAi} (v106683) stocks were
401 obtained from The Vienna *Drosophila* Stock Centre. The *Cyclin E-05306* stock was a kind gift from
402 Helena Richardson. The following stocks used in this study are described in the following references:
403 *MS1096-Gal4* (Capdevila & Guerrero, 1994), *ap-Gal4, (Calleja et al, 1996)*, and *UAS-Yki (Huang et*
404 *al., 2005)*.
405 Our *Drosophila* strains were raised on food that was made in-house containing agar (8g/L), brewer's
406 yeast (23.6g/L), dextrose (50.8g/L) and corn meal (58g/L). Depending on the experiment, flies were
407 housed in humidity-controlled incubators set at either 18°C or 25°C with a 12/12-hour light dark
408 cycle.
409

410 **List of Genotypes**

411 Figure 1
412 *(A) MS1096-Gal4, UAS-RFP/+; +/+; UAS-LacZ/+.*
413 (B-C) Control corresponds to *MS1096-Gal4, UAS-RFP/+; +/+; UAS-LacZ/+,*
414 *MS1096>dPGC1*^{RNAi} corresponds to *MS1096-Gal4, UAS-RFP/+; +/+; UAS-dPGC1*^{RNAi}*/+* and
415 *MS1096>dPGC1* corresponds to *MS1096-Gal4, UAS-RFP/+; +/+; EP-dPGC1/+.*
416

417 Figure 2
418 (A-H) Control corresponds to *ap-Gal4, UAS-CD8-GFP/+; tub-Gal80ts/UAS-LacZ,*
419 *ap>dPGC1*^{RNAi} corresponds to *ap-Gal4, UAS-CD8-GFP/+; tub-Gal80ts/UAS-dPGC1*^{RNAi}*,*
420 *ap>Yki* corresponds to *ap-Gal4, UAS-CD8-GFP/+; UAS-Yki, tub-Gal80ts/UAS-LacZ* and
421 *ap>Yki+dPGC1*^{RNAi} corresponds to *ap-Gal4, UAS-CD8-GFP/+; UAS-Yki, tub-Gal80ts/UAS-*
422 *dPGC1*^{RNAi}.
423

424 Figure 3

425 (A) The experimental condition corresponds to *ap-Gal4, UAS-CD8-GFP/+; UAS-Yki, tub-*
426 *Gal80ts/UAS-dPGC1*^{RNAi} and the control used for normalization corresponds to *ap-Gal4, UAS-*
427 *CD8-GFP/+; UAS-Yki, tub-Gal80ts/UAS-LacZ.*
428 (B) *ap-Gal4/+; UAS-Mito-GFP/+*
429 (C) *YW/+; +/+; Gug-Gal4, UAS-Mito-GFP/+*
430 (D) *Gug-Gal4, UAS-Mito-GFP/UAS-dMfn*
431 (E) *UAS-dMfn*^{RNAi}*/+; Gug-Gal4, UAS-Mito-GFP/+*
432 (F) *UAS-miro/+; Gug-Gal4, UAS-Mito-GFP/+*
433 (G) *UAS-miro*^{RNAi}*/+; Gug-Gal4, UAS-Mito-GFP/+*
434 (H-K) *ap>Yki* corresponds to *ap-Gal4, UAS-CD8-GFP/+; UAS-Yki, tub-Gal80ts/UAS-LacZ* and
435 *ap>Yki+dPGC1*^{RNAi} corresponds to *ap-Gal4, UAS-CD8-GFP/+; UAS-Yki, tub-Gal80ts/UAS-*
436 *dPGC1*^{RNAi}.
437
438 Figure 4
439 (A-I) Control corresponds to *ap-Gal4, UAS-CD8-GFP/+; tub-Gal80ts/UAS-LacZ, ap>Yki*
440 corresponds to *ap-Gal4, UAS-CD8-GFP/+; UAS-Yki, tub-Gal80ts/UAS-LacZ,*
441 *ap>Yki+dPGC1*^{RNAi} corresponds to *ap-Gal4, UAS-CD8-GFP/+; UAS-Yki, tub-Gal80ts/UAS-*
442 *dPGC1*^{RNAi}*, ap>Yki+dPGC1*^{RNAi}*+dMfn*^{RNAi} corresponds to *ap-Gal4, UAS-CD8-GFP/UAS-*
443 *dMfn*^{RNAi}*; UAS-Yki, tub-Gal80ts/UAS-dPGC1*^{RNAi}*, ap>Yki+dPGC1*^{RNAi}*+Opa1*^{RNAi} corresponds to
444 *ap-Gal4, UAS-CD8-GFP/UAS-dPGC1*^{shRNA}*; UAS-Yki, tub-Gal80ts/UAS-Opa1*^{RNAi}*,*
445 *ap>Yki+dMfn* corresponds to *ap-Gal4, UAS-CD8-GFP/+; UAS-Yki, tub-Gal80ts/UAS-dMfn* and
446 *ap>Yki+Opa1* corresponds to *ap-Gal4, UAS-CD8-GFP/EP-Opa1; UAS-Yki, tub-Gal80ts/+*
447
448 Figure 5
449 (A-B) Control corresponds to *ap-Gal4, UAS-CD8-GFP/+; tub-Gal80ts/UAS-LacZ, ap>Yki*
450 corresponds to *ap-Gal4, UAS-CD8-GFP/+; UAS-Yki, tub-Gal80ts/UAS-LacZ* and
451 *ap>Yki+dPGC1*^{RNAi} corresponds to *ap-Gal4, UAS-CD8-GFP/+; UAS-Yki, tub-Gal80ts/UAS-*
452 *dPGC1*^{RNAi}.
453 (C-N) Control corresponds to *ap-Gal4, UAS-CD8-GFP/+; tub-Gal80ts/UAS-LacZ, ap>cycE*^{mutant}
454 corresponds to *ap-Gal4, UAS-CD8-GFP/cycE*^{05306}*; tub-Gal80ts/+, ap>Yki* corresponds to *ap-*
455 *Gal4, UAS-CD8-GFP/+; UAS-Yki, tub-Gal80ts/UAS-LacZ, ap>Yki+dap*^{RNAi} corresponds to *ap-*
456 *Gal4, UAS-CD8-GFP/UAS- dap*^{RNAi}*; UAS-Yki, tub-Gal80ts/+, ap>Yki+dPGC1*^{RNAi} corresponds

457 to *ap-Gal4, UAS-CD8-GFP/+; UAS-Yki, tub-Gal80ts/UAS-dPGC1*^{RNAi} and
458 *ap>Yki+dPGC1*^{RNAi}*+cycE*^{mutant} corresponds to *ap-Gal4, UAS-CD8-GFP/cycE*^{05306}*; UAS-Yki,*
459 *tub-Gal80ts/UAS-dPGC1*^{RNAi}
460
461 Figure S1
462 (A-B) Control corresponds to *MS1096-Gal4, UAS-RFP/+; +/+; UAS-LacZ/+* and
463 *MS1096>dPGC1*^{shRNA} corresponds to *MS1096-Gal4, UAS-RFP/+; UAS-dPGC1*^{shRNA}*/+*.
464 *(B) MS1096>dPGC1*^{RNAi} corresponds to *MS1096-Gal4, UAS-RFP/+; +/+; UAS-dPGC1*^{RNAi}*/+,*
465 *MS1096>dPGC1*^{shRNA} corresponds to *MS1096-Gal4, UAS-RFP/+; UAS-dPGC1*^{shRNA}*/+* and
466 *MS1096>dPGC1* corresponds to *MS1096-Gal4, UAS-RFP/+; +/+; EP-dPGC-1/+*
467
468 Figure S2
469 (A-B) *ap-Gal4, UAS-CD8-GFP/UAS-dPGC1*^{shRNA}*; UAS-Yki, tub-Gal80ts/+*.
470 *(C)* Control corresponds to *ap-Gal4, UAS-CD8-GFP/+; tub-Gal80ts/UAS-LacZ, ap>dPGC1*^{shRNA}
471 corresponds to *ap-Gal4, UAS-CD8-GFP/ UAS-dPGC1*^{shRNA}*; tub-Gal80ts/+, ap>Yki*
472 corresponds to *ap-Gal4, UAS-CD8-GFP/+; UAS-Yki, tub-Gal80ts/UAS-LacZ* and
473 *ap>Yki+dPGC1*^{shRNA} corresponds to *ap-Gal4, UAS-CD8-GFP/UAS-dPGC1*^{shRNA}*; UAS-Yki,*
474 *tub-Gal80ts/+*
475
476 Figure S3
477 (A) Control corresponds to *YW/+; +/+; Gug-Gal4, UAS-Mito-GFP/+, Gug>dMfn* corresponds
478 to *Gug-Gal4, UAS-Mito-GFP/UAS-dMfn, Gug>Mfn*^{RNAi} corresponds to *UAS-dMfn*^{RNAi}*/+;*
479 *Gug-Gal4, UAS-Mito-GFP/+, Gug>miro* corresponds to *UAS-miro/+; Gug-Gal4, UAS-*
480 *Mito-GFP/+* and *Gug>miro*^{RNAi} corresponds to *UAS-miro*^{RNAi}*/+; Gug-Gal4, UAS-Mito-*
481 *GFP/+*
482
483 Figure S4
484 (A-F) Control corresponds to *ap-Gal4, UAS-CD8-GFP/+; tub-Gal80ts/UAS-LacZ, ap>Mfn*
485 corresponds to *ap-Gal4, UAS-CD8-GFP/+; tub-Gal80ts/ UAS-dMfn, ap>Mfn*^{RNAi} corresponds to
486 *ap-Gal4, UAS-CD8-GFP/ UAS-dMfn*^{RNAi}*; tub-Gal80ts/+, ap>Opa1* corresponds to *ap-Gal4,*
487 *UAS-CD8-GFP/EP-Opa1; tub-Gal80ts/+* and *ap>Opa1*^{RNAi} corresponds to *ap-Gal4, UAS-CD8-*
488 *GFP/+; tub-Gal80ts/ UAS-Opa1*^{RNAi}.

489

490 **Temporal control of transgene expression by Gal80^{TS}**

491 For experiments requiring the use of ap>Yki, the Gal4/Gal80^{TS} system was used to prevent lethality
492 during early development. This system allowed UAS-driven transgenes to be controlled in a
493 temperature-dependent manner. *Drosophila* crosses were kept for 2 days at 18°C to lay eggs. After 2
494 days, crosses were flipped into new vials and the old vials containing eggs were kept for 2 additional
495 days at 18°C before being transferred to a 29°C incubator for transgene expression to be induced. To
496 ensure that wing disc were analyzed at the same developmental stage, larvae with hyperplastic tumors
497 were dissected after 5 days at 29°C, whereas giant larvae containing neoplastic tumors were dissected
498 after 7 days at 29°C

499

500 **Immunohistochemistry**

501 Larvae were dissected in PBS and fixed in 3.7% formaldehyde / PBS for 20 mins at room temperature.
502 Samples were then washed in 0.2% triton / PBS (PBT) and blocked for an hour at room temperature
503 in blocking buffer (BBT) made of 0.2% triton, 5mM NaCl and 3% BSA diluted in PBS. Primary
504 antibodies were diluted in BBT, and the samples were left in primary antibody solution overnight at
505 room temperature. Longer primary antibody incubations were done at 4°C. After removing the
506 primary antibody and performing washes with BBT, samples were incubated for 2 hours at room
507 temperature with the relevant fluorescent secondary antibodies and DAPI that was diluted in BBT.
508 After removing the secondary antibody and performing washes with PBT. Samples were mounted in
509 90% glycerol / PBS containing 0.4% N-propyl gallate. BBT and PBT recipes were changed to 0.1%
510 tween instead of 0.1% triton for all stainings that were done for mitochondrial analysis.
511 The following primary antibodies were used: Anti-MMP1 (3A6B4/ 5H7B11/3B8D12 from
512 Developmental Studies Hybridoma Bank were mixed in equal volumes), Anti-pH2Av (Rockland
513 600-401-914, dilution 1:500). Secondary antibodies: DAPI (Invitrogen D1306, 60nM), Alexa Fluor
514 635 phalloidin was used to stain F-actin (Invitrogen A34054, dilution 1:200), Anti-mouse Alexa Fluor
515 555 (Invitrogen A21425, dilution 1:200), Anti-rabbit Alexa Fluor 555 (Invitrogen A21430, dilution
516 1:200).

517

518 **RNA extraction, cDNA synthesis, and Quantitative Polymerase Chain reaction (qPCR)**

519 Wing discs were dissected from *Drosophila* larvae and total RNA extracted by Trizol reagent (Life
520 Technologies, Ref: 15596026). RNA was treated with RQ1 DNase I (Promega, Ref: M6101) and
521 converted to cDNA using the SuperScript III Reverse Transcriptase kit (Life technologies, Ref:

522 18080-044). Real-time PCR quantification was performed using 5x HOT FIREpol EvaGreen qPCR
523 Mix Plus (Solis BiodDyne, Ref: 08-24-00001) on the QuantStudio 6 Flex Real-Time PCR machine
524 (Applied Biosystem). Table 1 contains the sequence of all the primers used for our experiments.
525
526 **List of primers**

Gene	Forward primer sequence:	Reverse primer sequence:
dPGC1	GCTGACTTGGATAATGCTGGCA	TGAACCTACCGGTGACTTGC
TFAM	AACAAAGTCAGGCCCCTAGC	CCGCATGAAGCGAAAGTAGG
dERR	GGAATTGGTCAGCGTCATTGG	GAACTCCGTGTAACCGCACT
Ets97D	GGTGCCCTGGAAGAAGTGATT	ACGCATTGGTCCACGAGATT
ewg	CGATGTTGATTACACCACGCA	TTTGAATGGTAGCACCGCCT
dMfn	AGCAGTATTGGACACAGCGT	ACGCCAGCCGATAGTTTTCA
Opa1	CCCATGAAGGCTTTGGGCTA	ACCCCTCGACGATGGAAAAG
Drp1	AGATGCTGCGCTTTCCCAAA	AGTAGGGATCGCTGTCCGTT
Pink1	TACCGACAGGACCAATTGCC	CCACTGTAGGATCTCCGGACT
Park	CGGATGTGAGTGATACCGTGT	TACTCCTCGCGTGTCAACAG
Atg7	GTGACACGACCCGGAGTATC	ATTTAGGACGGCCGCTGAAC
milt	AAGGACCTAGAGCTGACCGT	GGAGTGTCAGTATCTGTGCCA
miro	TATTCCACCATGGACAGCGT	CGGATGTGAGCTCCTGTTCTTC
Cyclin E	TTCTACCAGCAGCACTGAGC	TGGAAGGATAGCGATTGGGC
Rp49	AAGCGGCGACGCACTCTGTT	GCCCAGCATACAGGCCCAAG

527
528 **qPCR statistics**
529 All qPCR experiments to check gene expression were performed a minimum of three times
530 (independent experiments) on several wing discs for Figs. 3A, 5B and S1C (total number are indicated
531 in the figures legends). Statistical analysis was done using GraphPad Prism, values were checked if
532 they were normally distributed using the Shapiro-Wilk test. If normally distributed, statistical
533 significance was determined using Unpaired t-test with Welch's correction, if not, statistical
534 significance was determined by Mann-Whitney test.
535
536 **Western blot**
537 Wing discs were dissected from *Drosophila* larvae and transferred into RIPA protein extraction and
538 immunoprecipitation buffer (Sigma-Aldrich, Ref: R0278) containing cOmplete Protease Inhibitor
539 Cocktail (Merck, Ref: 04693124001), PhosSTOP (Merck, Ref: 04906837001) and 100mM PMSF
540 stock (Sigma-Aldrich, Ref: 93482). The wing discs were homogenized by pipetting the sample up
541 and down and then leaving the sample on ice for 30 mins. After 30 mins, the samples were sonicated

542 3 times for 3 cycles with the following settings: 100% amplitude, 1 cycle. The samples were then
543 centrifuged for 20 mins, 15000g at 4°C to obtain the supernatant that was used for our western blots.
544 Protein quantification was performed using The Pierce BCA protein assay kit (Thermo Fisher
545 Scientific, Ref: 23227). 15 µg of protein was loaded for each sample for the Western blots. Western
546 blot membranes were blocked for an hour at room temperature with 5% skimmed milk (Fluka, Ref:
547 70166-500G) dissolved in TBST. After washing with TBST, the membranes were incubated
548 overnight at 4°C with primary antibodies that were diluted in TBST. After removing the primary
549 antibody and performing washes with TBST, samples were incubated for 1 hours at room temperature
550 with the relevant secondary HRP antibodies. After removing the secondary antibodies and performing
551 washes with TBST. The Pierce ECL Western Blotting Substrate kit (Thermo Fisher Scientific, Ref:
552 32106) was used to visualize protein levels on the Amersham Imager 600 (GE healthcare).
553 The following primary antibodies were used: Anti cyclin E (sc-33748, dilution 1:1000) and 12G10
554 anti-alpha-tubulin (DSHB AB_1157911, dilution 1:1000). HRP Secondary antibodies: Polyclonal
555 goat anti rabbit HRP (Dako P0448, dilution 1:5000) and Polyclonal goat anti mouse HRP (Dako
556 P0447, dilution 1:5000)
557
558 **Electron microscopy**
559 Larval wing disc and tumors were dissected in PBS and fixed in 2% glutaraldehyde / 0.1M sodium
560 cacodylate buffer at room temperature. Samples were then passed to staff of the Core Facility for
561 Integrative Microscopy at The University of Copenhagen, so that thin sections of tissue could be cut
562 and prepared for imaging. All specimens were imaged by either our collaborators or staff at the Core
563 Facility for Integrative Microscopy. Images were acquired with a Transmission Electron Microscope
564 Philips CM100, FEL.
565
566 **Imaging and quantification of *Drosophila* wing imaginal disc size**
567 Confocal images of *Drosophila* wing imaginal disc were acquired with a Leica SP8 confocal laser-
568 scanning microscope and processed with ImageJ software. The area of the wing disc expressing our
569 transgenes of interest was determined using ImageJ. Using the 'threshold' function, we set the
570 threshold to only the GFP-positive area of the wing disc. Next, we used the 'Analyze particles' option
571 to quantify the area size. For every genotype, a minimum of 10 discs were quantified. Using GraphPad
572 Prism, values were checked if they were normally distributed using the D'Agostino and Pearson test.

573 If normally distributed, statistical significance was determined using Unpaired t-test with Welch's
574 correction, if not, statistical significance was determined by Mann-Whitney test.
575
576 **Imaging and quantification of *Drosophila* adult wing size**
577 Images of adult *Drosophila* wings were taken with a Leica M165 stereomicroscope and processed
578 with ImageJ software. Crosses were allowed to lay eggs on apple agar plates with yeast paste at 25°C
579 for 10 to 14 hours. Once eggs hatch and L1 larvae emerge, 20 larvae were transferred to vials
580 containing standard *Drosophila* food, these vials were kept at 29°C until adult flies eclose. To fix the
581 wings, adult flies were soaked in a 25% glycerol, 75% ethanol mixture for at least 24 hours, after that,
582 the wings were plucked and mounted in glycerol for imaging. To measure the wing area, the polygon
583 selection tool in ImageJ was used to draw a boarder around the edges of the wing. Next the 'measure'
584 option was used to quantify the area size. For every genotype, 20 wings were quantified. Using
585 GraphPad Prism, values were checked if they were normally distributed using the D'Agostino and
586 Pearson test and statistical significance was determined using Unpaired t-test with Welch's
587 correction.
588
589 **Quantification of mitochondria size in peripodial membrane**
590 The Gug-Gal4 driver was used to drive the expression of the Mito-GFP mitochondria marker in the
591 peripodial membrane. Two filters were applied to the images: unsharp mask (radius = 10.0 pixels,
592 mask strength = 0.9) and median filtering (radius = 3) to enhance and smooth the Mito-GFP signal
593 respectively (Terriente-Felix, A. et al, 2020). Next, the 'threshold' function was used to create a
594 binary mask and the Mitochondrial analyzer 2D analysis plugin from ImageJ (Chaudhry, A., 2019)
595 was used to calculate the mean form factor. For every genotype, mitochondria from a minimum of
596 15 images were quantified. Using GraphPad Prism, values were checked if they were normally
597 distributed using the D'Agostino and Pearson test. If normally distributed, statistical significance was
598 determined using Unpaired t-test with Welch's correction, if not, statistical significance was
599 determined by Mann-Whitney test.

Acknowledgements

We thank Helena Richardson for reagents. We thank Bloomington Drosophila Stock Center, Vienna Drosophila Resource Center, and FlyORF, for fly stocks; Developmental Studies Hybridoma Bank for antibodies; and the fly community for sharing reagents.

Conflict of interest

The authors declare that the research was conducted in the absence of any commercial or financial relationships that could be construed as a potential conflict of interest.

Funding

This work was supported by the Independent Research Fund Denmark Grant 0134-00045B, Novo Nordisk Foundation Grant NNF18OC0052223, a grant from the Neye Foundation, and a grant from Grosserer Alfred Nielsen og Hustru's fond.

614 ## References

615

616 Adebayo M, Singh S, Singh AP, Dasgupta S (2021) Mitochondrial fusion and fission: The fine-tune
617 balance for cellular homeostasis. *FASEB J* 35: e21620

618 Antico Arciuch VG, Elguero ME, Poderoso JJ, Carreras MC (2012) Mitochondrial regulation of cell
619 cycle and proliferation. *Antioxid Redox Signal* 16: 1150-1180

620 Arany Z, He H, Lin J, Hoyer K, Handschin C, Toka O, Ahmad F, Matsui T, Chin S, Wu PH *et al* (2005)
621 Transcriptional coactivator PGC-1 alpha controls the energy state and contractile function of cardiac
622 muscle. *Cell metabolism* 1: 259-271

623 Archer SL (2013) Mitochondrial dynamics--mitochondrial fission and fusion in human diseases. *N*
624 *Engl J Med* 369: 2236-2251

625 Baltzer C, Tiefenbock SK, Marti M, Frei C (2009) Nutrition controls mitochondrial biogenesis in the
626 Drosophila adipose tissue through Delg and cyclin D/Cdk4. *PLoS One* 4: e6935

627 Bandura JL, Edgar BA (2008) Yorkie and Scalloped: partners in growth activation. *Dev Cell* 14: 315-
628 316

629 Barron DA, Kagey JD (2014) The role of the Hippo pathway in human disease and tumorigenesis. *Clin*
630 *Transl Med* 3: 25

631 Beaucher M, Hersperger E, Page-McCaw A, Shearn A (2007) Metastatic ability of Drosophila tumors
632 depends on MMP activity. *Dev Biol* 303: 625-634

633 Besson A, Dowdy SF, Roberts JM (2008) CDK inhibitors: cell cycle regulators and beyond. *Dev Cell*
634 14: 159-169

635 Bhalla K, Hwang BJ, Dewi RE, Ou L, Twaddel W, Fang HB, Vafai SB, Vazquez F, Puigserver P, Boros L
636 *et al* (2011) PGC1alpha promotes tumor growth by inducing gene expression programs supporting
637 lipogenesis. *Cancer Res* 71: 6888-6898

638 Blackford AN, Jackson SP (2017) ATM, ATR, and DNA-PK: The Trinity at the Heart of the DNA Damage
639 Response. *Mol Cell* 66: 801-817

640 Brand AH, Perrimon N (1993) Targeted gene expression as a means of altering cell fates and
641 generating dominant phenotypes. *Development* 118: 401-415

642 Calleja M, Moreno E, Pelaz S, Morata G (1996) Visualization of gene expression in living adult
643 Drosophila. *Science* 274: 252-255

644 Calses PC, Crawford JJ, Lill JR, Dey A (2019) Hippo Pathway in Cancer: Aberrant Regulation and
645 Therapeutic Opportunities. *Trends Cancer* 5: 297-307

646 Capdevila J, Guerrero I (1994) Targeted expression of the signaling molecule decapentaplegic
647 induces pattern duplications and growth alterations in Drosophila wings. *The EMBO journal* 13:
648 4459-4468

649 Chan DC (2020) Mitochondrial Dynamics and Its Involvement in Disease. *Annu Rev Pathol* 15: 235-
650 259

651 Chen J, Shi X, Padmanabhan R, Wang Q, Wu Z, Stevenson SC, Hild M, Garza D, Li H (2008)
652 Identification of novel modulators of mitochondrial function by a genome-wide RNAi screen in
653 Drosophila melanogaster. *Genome Res* 18: 123-136

654 Chen S, Oliveira MT, Sanz A, Kemppainen E, Fukuoh A, Schlicht B, Kaguni LS, Jacobs HT (2012) A
655 cytoplasmic suppressor of a nuclear mutation affecting mitochondrial functions in Drosophila.
656 *Genetics* 192: 483-493

657 Dai W, Jiang L (2019) Dysregulated Mitochondrial Dynamics and Metabolism in Obesity, Diabetes,
658 and Cancer. *Front Endocrinol (Lausanne)* 10: 570

659 de Nooij JC, Letendre MA, Hariharan IK (1996) A cyclin-dependent kinase inhibitor, Dacapo, is
660 necessary for timely exit from the cell cycle during Drosophila embryogenesis. *Cell* 87: 1237-1247

661 Dekanty A, Barrio L, Milan M (2015) Contributions of DNA repair, cell cycle checkpoints and cell
662 death to suppressing the DNA damage-induced tumorigenic behavior of Drosophila epithelial cells.
663 *Oncogene* 34: 978-985

664 Deng H, Dodson MW, Huang H, Guo M (2008) The Parkinson's disease genes pink1 and parkin
665 promote mitochondrial fission and/or inhibit fusion in Drosophila. *Proc Natl Acad Sci U S A* 105:
666 14503-14508

667 Ding L, Lei Y, Han Y, Li Y, Ji X, Liu L (2016) Vimar Is a Novel Regulator of Mitochondrial Fission through
668 Miro. *PLoS Genet* 12: e1006359

669 Diop SB, Bisharat-Kernizan J, Birse RT, Oldham S, Ocorr K, Bodmer R (2015) PGC-1/Spargel
670 Counteracts High-Fat-Diet-Induced Obesity and Cardiac Lipotoxicity Downstream of TOR and
671 Brummer ATGL Lipase. *Cell Rep* 10: 1572-1584

672 Dubal D, Moghe P, Verma RK, Uttekar B, Rikhy R (2022) Mitochondrial fusion regulates proliferation
673 and differentiation in the type II neuroblast lineage in Drosophila. *PLoS Genet* 18: e1010055

674 Ekholm-Reed S, Mendez J, Tedesco D, Zetterberg A, Stillman B, Reed SI (2004) Deregulation of cyclin
675 E in human cells interferes with prereplication complex assembly. *J Cell Biol* 165: 789-800

676 Enomoto M, Kizawa D, Ohsawa S, Igaki T (2015) JNK signaling is converted from anti- to pro-tumor
677 pathway by Ras-mediated switch of Warts activity. *Dev Biol* 403: 162-171

678 Feilchenfeldt J, Brundler MA, Soravia C, Totsch M, Meier CA (2004) Peroxisome proliferator-
679 activated receptors (PPARs) and associated transcription factors in colon cancer: reduced
680 expression of PPARgamma-coactivator 1 (PGC-1). *Cancer Lett* 203: 25-33

681 Fernandez-Capetillo O, Celeste A, Nussenzweig A (2003) Focusing on foci: H2AX and the recruitment
682 of DNA-damage response factors. *Cell Cycle* 2: 426-427

683 Fernandez BG, Gaspar P, Bras-Pereira C, Jezowska B, Rebelo SR, Janody F (2011) Actin-Capping
684 Protein and the Hippo pathway regulate F-actin and tissue growth in Drosophila. *Development* 138:
685 2337-2346

686 Fernandez BG, Jezowska B, Janody F (2014) Drosophila actin-Capping Protein limits JNK activation
687 by the Src proto-oncogene. *Oncogene* 33: 2027-2039

688 Finkel T, Hwang PM (2009) The Krebs cycle meets the cell cycle: mitochondria and the G1-S
689 transition. *Proc Natl Acad Sci U S A* 106: 11825-11826

690 Gaillard H, Garcia-Muse T, Aguilera A (2015) Replication stress and cancer. *Nat Rev Cancer* 15: 276-
691 289

692 Garcez M, Branco-Santos J, Gracio PC, Homem CCF (2020) Mitochondrial Dynamics in the Drosophila
693 Ovary Regulates Germ Stem Cell Number, Cell Fate, and Female Fertility. *Front Cell Dev Biol* 8:
694 596819

695 George J, Jacobs HT (2019) Germline knockdown of spargel (PGC-1) produces embryonic lethality in
696 Drosophila. *Mitochondrion* 49: 189-199

697 Gerlach SU, Eichenlaub T, Herranz H (2018) Yorkie and JNK Control Tumorigenesis in Drosophila Cells
698 with Cytokinesis Failure. *Cell Rep* 23: 1491-1503

699 Gerlach SU, Herranz H (2020) Genomic instability and cancer: lessons from Drosophila. *Open Biol*
700 10: 200060

701 Gerlach SU, Sander M, Song S, Herranz H (2019) The miRNA bantam regulates growth and
702 tumorigenesis by repressing the cell cycle regulator tribbles. *Life Sci Alliance* 2

703 Gershman B, Puig O, Hang L, Peitzsch RM, Tatar M, Garofalo RS (2007) High-resolution dynamics of
704 the transcriptional response to nutrition in Drosophila: a key role for dFOXO. *Physiol Genomics* 29:
705 24-34

706 Gibson MC, Lehman DA, Schubiger G (2002) Lumenal transmission of decapentaplegic in Drosophila
707 imaginal discs. *Dev Cell* 3: 451-460

708 Gibson MC, Schubiger G (2001) Drosophila peripodial cells, more than meets the eye? *Bioessays* 23:
709 691-697

710 Girnun GD (2012) The diverse role of the PPARγ coactivator 1 family of transcriptional coactivators
711 in cancer. *Seminars in cell & developmental biology* 23: 381-388

712 Gonzalez C (2013) Drosophila melanogaster: a model and a tool to investigate malignancy and
713 identify new therapeutics. *Nat Rev Cancer* 13: 172-183

714 Guo X, Macleod GT, Wellington A, Hu F, Panchumarthi S, Schoenfield M, Marin L, Charlton MP,
715 Atwood HL, Zinsmaier KE (2005) The GTPase dMiro is required for axonal transport of mitochondria
716 to Drosophila synapses. *Neuron* 47: 379-393

717 Halazonetis TD, Gorgoulis VG, Bartek J (2008) An oncogene-induced DNA damage model for cancer
718 development. *Science (New York, NY)* 319: 1352-1355

719 Hanahan D (2022) Hallmarks of Cancer: New Dimensions. *Cancer Discov* 12: 31-46

720 Hanahan D, Weinberg RA (2011) Hallmarks of cancer: the next generation. *Cell* 144: 646-674

721 Herranz H, Eichenlaub T, Cohen SM (2016) Cancer in Drosophila: Imaginal Discs as a Model for
722 Epithelial Tumor Formation. *Current topics in developmental biology* 116: 181-199

723 Horbay R, Bilyy R (2016) Mitochondrial dynamics during cell cycling. *Apoptosis* 21: 1327-1335

724 Huang J, Wu S, Barrera J, Matthews K, Pan D (2005) The Hippo signaling pathway coordinately
725 regulates cell proliferation and apoptosis by inactivating Yorkie, the Drosophila Homolog of YAP.
726 *Cell* 122: 421-434

727 Igaki T, Pagliarini RA, Xu T (2006) Loss of cell polarity drives tumor growth and invasion through JNK
728 activation in Drosophila. *Current biology : CB* 16: 1139-1146

729 Jones AW, Yao Z, Vicencio JM, Karkucinska-Wieckowska A, Szabadkai G (2012) PGC-1 family
730 coactivators and cell fate: roles in cancer, neurodegeneration, cardiovascular disease and
731 retrograde mitochondria-nucleus signalling. *Mitochondrion* 12: 86-99

732 Khoo P, Allan K, Willoughby L, Brumby AM, Richardson HE (2013) In Drosophila, RhoGEF2 cooperates
733 with activated Ras in tumorigenesis through a pathway involving Rho1-Rok-Myosin-II and JNK
734 signalling. *Dis Model Mech* 6: 661-678

735 Koo JH, Guan KL (2018) Interplay between YAP/TAZ and Metabolism. *Cell metabolism* 28: 196-206

736 Kowalczyk W, Romanelli L, Atkins M, Hillen H, Bravo Gonzalez-Blas C, Jacobs J, Xie J, Soheily S,
737 Verboven E, Moya IM *et al* (2022) Hippo signaling instructs ectopic but not normal organ growth.
738 *Science* 378: eabg3679

739 La Marca JE, Richardson HE (2020) Two-Faced: Roles of JNK Signalling During Tumourigenesis in the
740 Drosophila Model. *Front Cell Dev Biol* 8: 42

741 Lane ME, Sauer K, Wallace K, Jan YN, Lehner CF, Vaessin H (1996) Dacapo, a cyclin-dependent kinase
742 inhibitor, stops cell proliferation during Drosophila development. *Cell* 87: 1225-1235

743 LeBleu VS, O'Connell JT, Gonzalez Herrera KN, Wikman H, Pantel K, Haigis MC, de Carvalho FM,
744 Damascena A, Domingos Chinen LT, Rocha RM *et al* (2014) PGC-1alpha mediates mitochondrial
745 biogenesis and oxidative phosphorylation in cancer cells to promote metastasis. *Nat Cell Biol* 16:
746 992-1003, 1001-1015

747 Lee KS, Lu B (2014) The myriad roles of Miro in the nervous system: axonal transport of mitochondria
748 and beyond. *Front Cell Neurosci* 8: 330

749 Lelliott CJ, Medina-Gomez G, Petrovic N, Kis A, Feldmann HM, Bjursell M, Parker N, Curtis K,
750 Campbell M, Hu P *et al* (2006) Ablation of PGC-1beta results in defective mitochondrial activity,
751 thermogenesis, hepatic function, and cardiac performance. *PLoS Biol* 4: e369

752 Leone TC, Lehman JJ, Finck BN, Schaeffer PJ, Wende AR, Boudina S, Courtois M, Wozniak DF,
753 Sambandam N, Bernal-Mizrachi C *et al* (2005) PGC-1alpha deficiency causes multi-system energy
754 metabolic derangements: muscle dysfunction, abnormal weight control and hepatic steatosis. *PLoS*
755 *Biol* 3: e101

756 Liao JZ, Chung HL, Shih C, Wong KKL, Dutta D, Nil Z, Burns CG, Kanca O, Park YJ, Zuo Z *et al* (2024)
757 Cdk8/CDK19 promotes mitochondrial fission through Drp1 phosphorylation and can phenotypically
758 suppress pink1 deficiency in Drosophila. *Nat Commun* 15: 3326

759 Lin J, Wu PH, Tarr PT, Lindenberg KS, St-Pierre J, Zhang CY, Mootha VK, Jager S, Vianna CR, Reznick
760 RM *et al* (2004) Defects in adaptive energy metabolism with CNS-linked hyperactivity in PGC-1alpha
761 null mice. *Cell* 119: 121-135

762 Liu X, Hajnoczky G (2009) Ca2+-dependent regulation of mitochondrial dynamics by the Miro-Milton
763 complex. *Int J Biochem Cell Biol* 41: 1972-1976

764 Lopez-Mejia IC, Fajas L (2015) Cell cycle regulation of mitochondrial function. *Current opinion in cell*
765 *biology* 33: 19-25

766 Ma Y, Wang L, Jia R (2020) The role of mitochondrial dynamics in human cancers. *Am J Cancer Res*
767 10: 1278-1293

768 Mandal S, Guptan P, Owusu-Ansah E, Banerjee U (2005) Mitochondrial regulation of cell cycle
769 progression during development as revealed by the tenured mutation in Drosophila. *Dev Cell* 9: 843-
770 854

771 Mishra P, Chan DC (2014) Mitochondrial dynamics and inheritance during cell division, development
772 and disease. *Nat Rev Mol Cell Biol* 15: 634-646

773 Misra S, Pandey AK, Gupta S, Kumar A, Khanna P, Shankar J, Ravi Ram K (2017) Estrogen related
774 receptor is required for the testicular development and for the normal sperm
775 axoneme/mitochondrial derivatives in Drosophila males. *Sci Rep* 7: 40372

776 Mitra K (2013) Mitochondrial fission-fusion as an emerging key regulator of cell proliferation and
777 differentiation. *Bioessays* 35: 955-964

778 Mitra K, Rikhy R, Lilly M, Lippincott-Schwartz J (2012) DRP1-dependent mitochondrial fission
779 initiates follicle cell differentiation during Drosophila oogenesis. *J Cell Biol* 197: 487-497

780 Mitra K, Wunder C, Roysam B, Lin G, Lippincott-Schwartz J (2009) A hyperfused mitochondrial state
781 achieved at G1-S regulates cyclin E buildup and entry into S phase. *Proc Natl Acad Sci U S A* 106:
782 11960-11965

783 Molano-Fernandez M, Hickson ID, Herranz H (2022) Cyclin E overexpression in the Drosophila
784 accessory gland induces tissue dysplasia. *Front Cell Dev Biol* 10: 992253

785 Moon S, Yeon Park S, Woo Park H (2018) Regulation of the Hippo pathway in cancer biology. *Cell*
786 *Mol Life Sci* 75: 2303-2319

787 Mouchiroud L, Eichner LJ, Shaw RJ, Auwerx J (2014) Transcriptional coregulators: fine-tuning
788 metabolism. *Cell metabolism* 20: 26-40

789 Mukherjee S, Basar MA, Davis C, Duttaroy A (2014) Emerging functional similarities and divergences
790 between Drosophila Spargel/dPGC-1 and mammalian PGC-1 protein. *Frontiers in genetics* 5: 216

791 Mukherjee S, Duttaroy A (2013) Spargel/dPGC-1 is a new downstream effector in the insulin-TOR
792 signaling pathway in Drosophila. *Genetics* 195: 433-441

793 Nagaraj R, Gururaja-Rao S, Jones KT, Slattery M, Negre N, Braas D, Christofk H, White KP, Mann R,
794 Banerjee U (2012) Control of mitochondrial structure and function by the Yorkie/YAP oncogenic
795 pathway. *Genes & development* 26: 2027-2037

796 Narendra DP, Jin SM, Tanaka A, Suen DF, Gautier CA, Shen J, Cookson MR, Youle RJ (2010) PINK1 is
797 selectively stabilized on impaired mitochondria to activate Parkin. *PLoS Biol* 8: e1000298

798 Nolo R, Morrison CM, Tao C, Zhang X, Halder G (2006) The bantam microRNA is a target of the hippo
799 tumor-suppressor pathway. *Current biology : CB* 16: 1895-1904

800 Owusu-Ansah E, Yavari A, Mandal S, Banerjee U (2008) Distinct mitochondrial retrograde signals
801 control the G1-S cell cycle checkpoint. *Nature genetics* 40: 356-361

802 Panchal K, Tiwari AK (2020) Miro, a Rho GTPase genetically interacts with Alzheimer's disease-
803 associated genes (Tau, Abeta42 and Appl) in Drosophila melanogaster. *Biol Open* 9

804 Pavlova NN, Thompson CB (2016) The Emerging Hallmarks of Cancer Metabolism. *Cell metabolism*
805 23: 27-47

806 Picard M, Shirihai OS, Gentil BJ, Burelle Y (2013) Mitochondrial morphology transitions and
807 functions: implications for retrograde signaling? *Am J Physiol Regul Integr Comp Physiol* 304: R393-
808 406

809 Pinal N, Calleja M, Morata G (2019) Pro-apoptotic and pro-proliferation functions of the JNK
810 pathway of Drosophila: roles in cell competition, tumorigenesis and regeneration. *Open Biol* 9:
811 180256

812 Qian L, Zhu Y, Deng C, Liang Z, Chen J, Chen Y, Wang X, Liu Y, Tian Y, Yang Y (2024) Peroxisome
813 proliferator-activated receptor gamma coactivator-1 (PGC-1) family in physiological and
814 pathophysiological process and diseases. *Signal Transduct Target Ther* 9: 50

815 Qian W, Choi S, Gibson GA, Watkins SC, Bakkenist CJ, Van Houten B (2012) Mitochondrial
816 hyperfusion induced by loss of the fission protein Drp1 causes ATM-dependent G2/M arrest and
817 aneuploidy through DNA replication stress. *J Cell Sci* 125: 5745-5757

818 Rai M, Katti P, Nongthomba U (2014) Drosophila Erect wing (Ewg) controls mitochondrial fusion
819 during muscle growth and maintenance by regulation of the Opa1-like gene. *J Cell Sci* 127: 191-203

820 Rera M, Bahadorani S, Cho J, Koehler CL, Ulgherait M, Hur JH, Ansari WS, Lo T, Jr., Jones DL, Walker
821 DW (2011) Modulation of longevity and tissue homeostasis by the Drosophila PGC-1 homolog. *Cell*
822 *metabolism* 14: 623-634

823 Rizzuto R, Brini M, Pizzo P, Murgia M, Pozzan T (1995) Chimeric green fluorescent protein as a tool
824 for visualizing subcellular organelles in living cells. *Current biology : CB* 5: 635-642

825 Rogers RP, Rogina B (2014) Increased mitochondrial biogenesis preserves intestinal stem cell
826 homeostasis and contributes to longevity in Indy mutant flies. *Aging (Albany NY)* 6: 335-350

827 Satyanarayana A, Kaldis P (2009) Mammalian cell-cycle regulation: several Cdks, numerous cyclins
828 and diverse compensatory mechanisms. *Oncogene* 28: 2925-2939

829 Saxena S, Zou L (2022) Hallmarks of DNA replication stress. *Mol Cell* 82: 2298-2314

830 Scarpulla RC (2011) Metabolic control of mitochondrial biogenesis through the PGC-1 family
831 regulatory network. *Biochimica et biophysica acta* 1813: 1269-1278

832 Senft D, Ronai ZA (2016) Regulators of mitochondrial dynamics in cancer. *Current opinion in cell*
833 *biology* 39: 43-52

834 Shu Z, Deng WM (2017) Differential Regulation of Cyclin E by Yorkie-Scalloped Signaling in Organ
835 Development. *G3 (Bethesda)* 7: 1049-1060

836 Siu KT, Rosner MR, Minella AC (2012) An integrated view of cyclin E function and regulation. *Cell*
837 *Cycle* 11: 57-64

838 Sonoda J, Mehl IR, Chong LW, Nofsinger RR, Evans RM (2007) PGC-1beta controls mitochondrial
839 metabolism to modulate circadian activity, adaptive thermogenesis, and hepatic steatosis. *Proc Natl*
840 *Acad Sci U S A* 104: 5223-5228

841 Spruck CH, Won KA, Reed SI (1999) Deregulated cyclin E induces chromosome instability. *Nature*
842 401: 297-300

843 Stowers RS, Megeath LJ, Górska-Andrzejak J, Meinertzhagen IA, Schwarz TL (2002) Axonal transport
844 of mitochondria to synapses depends on milton, a novel Drosophila protein. *Neuron* 36: 1063-1077

845 Sullivan LB, Gui DY, Vander Heiden MG (2016) Altered metabolite levels in cancer: implications for
846 tumour biology and cancer therapy. *Nat Rev Cancer* 16: 680-693

847 Takata K, Yoshida H, Hirose F, Yamaguchi M, Kai M, Oshige M, Sakimoto I, Koiwai O, Sakaguchi K
848 (2001) Drosophila mitochondrial transcription factor A: characterization of its cDNA and expression
849 pattern during development. *Biochem Biophys Res Commun* 287: 474-483

850 Tan Z, Luo X, Xiao L, Tang M, Bode AM, Dong Z, Cao Y (2016) The Role of PGC1alpha in Cancer
851 Metabolism and its Therapeutic Implications. *Molecular cancer therapeutics* 15: 774-782

852 Tang BL (2015) MIRO GTPases in Mitochondrial Transport, Homeostasis and Pathology. *Cells* 5

853 Tapon N, Harvey KF, Bell DW, Wahrer DC, Schiripo TA, Haber D, Hariharan IK (2002) salvador
854 Promotes both cell cycle exit and apoptosis in Drosophila and is mutated in human cancer cell lines.
855 *Cell* 110: 467-478

856 Thompson BJ, Cohen SM (2006) The Hippo pathway regulates the bantam microRNA to control cell
857 proliferation and apoptosis in Drosophila. *Cell* 126: 767-774

858 Tiefenböck SK, Baltzer C, Egli NA, Frei C (2010) The Drosophila PGC-1 homologue Spargel coordinates
859 mitochondrial activity to insulin signalling. *The EMBO journal* 29: 171-183

860 Torrano V, Valcarcel-Jimenez L, Cortazar AR, Liu X, Urosevic J, Castillo-Martin M, Fernandez-Ruiz S,
861 Morciano G, Caro-Maldonado A, Guiu M *et al* (2016) The metabolic co-regulator PGC1alpha
862 suppresses prostate cancer metastasis. *Nat Cell Biol* 18: 645-656

863 Tubbs A, Nussenzweig A (2017) Endogenous DNA Damage as a Source of Genomic Instability in
864 Cancer. *Cell* 168: 644-656

865 Uhlirova M, Bohmann D (2006) JNK- and Fos-regulated Mmp1 expression cooperates with Ras to
866 induce invasive tumors in Drosophila. *The EMBO journal* 25: 5294-5304

867 Varelas X (2014) The Hippo pathway effectors TAZ and YAP in development, homeostasis and
868 disease. *Development* 141: 1614-1626

869 Vianna CR, Huntgeburth M, Coppari R, Choi CS, Lin J, Krauss S, Barbatelli G, Tzameli I, Kim YB, Cinti
870 S *et al* (2006) Hypomorphic mutation of PGC-1beta causes mitochondrial dysfunction and liver
871 insulin resistance. *Cell metabolism* 4: 453-464

872 Villena JA (2015) New insights into PGC-1 coactivators: redefining their role in the regulation of
873 mitochondrial function and beyond. *The FEBS journal* 282: 647-672

874 Vincow ES, Merrihew G, Thomas RE, Shulman NJ, Beyer RP, MacCoss MJ, Pallanck LJ (2013) The
875 PINK1-Parkin pathway promotes both mitophagy and selective respiratory chain turnover in vivo.
876 *Proc Natl Acad Sci U S A* 110: 6400-6405

877 Vyas S, Zaganjor E, Haigis MC (2016) Mitochondria and Cancer. *Cell* 166: 555-566

878 Wang Y, Peng J, Yang D, Xing Z, Jiang B, Ding X, Jiang C, Ouyang B, Su L (2024) From metabolism to
879 malignancy: the multifaceted role of PGC1alpha in cancer. *Front Oncol* 14: 1383809

880 Watkins G, Douglas-Jones A, Mansel RE, Jiang WG (2004) The localisation and reduction of nuclear
881 staining of PPARgamma and PGC-1 in human breast cancer. *Oncol Rep* 12: 483-488

882 Yao CH, Wang R, Wang Y, Kung CP, Weber JD, Patti GJ (2019) Mitochondrial fusion supports
883 increased oxidative phosphorylation during cell proliferation. *eLife* 8

884 Yu FX, Zhao B, Guan KL (2015) Hippo Pathway in Organ Size Control, Tissue Homeostasis, and Cancer.
885 *Cell* 163: 811-828

886 Yu K, Ramkumar N, Wong KKL, Tettweiler G, Verheyen EM (2023) The AMPK-like protein kinases
887 Sik2 and Sik3 interact with Hipk and induce synergistic tumorigenesis in a Drosophila cancer model.
888 *Front Cell Dev Biol* 11: 1214539

889 Zhang Y, Ba Y, Liu C, Sun G, Ding L, Gao S, Hao J, Yu Z, Zhang J, Zen K *et al* (2007) PGC-1alpha induces
890 apoptosis in human epithelial ovarian cancer cells through a PPARgamma-dependent pathway. *Cell*
891 *Res* 17: 363-373

892 Zheng Y, Pan D (2019) The Hippo Signaling Pathway in Development and Disease. *Dev Cell* 50: 264-
893 282

894 Zorzano A, Liesa M, Sebastian D, Segales J, Palacin M (2010) Mitochondrial fusion proteins: dual
895 regulators of morphology and metabolism. *Seminars in cell & developmental biology* 21: 566-574

896

897

898 **FIGURES**

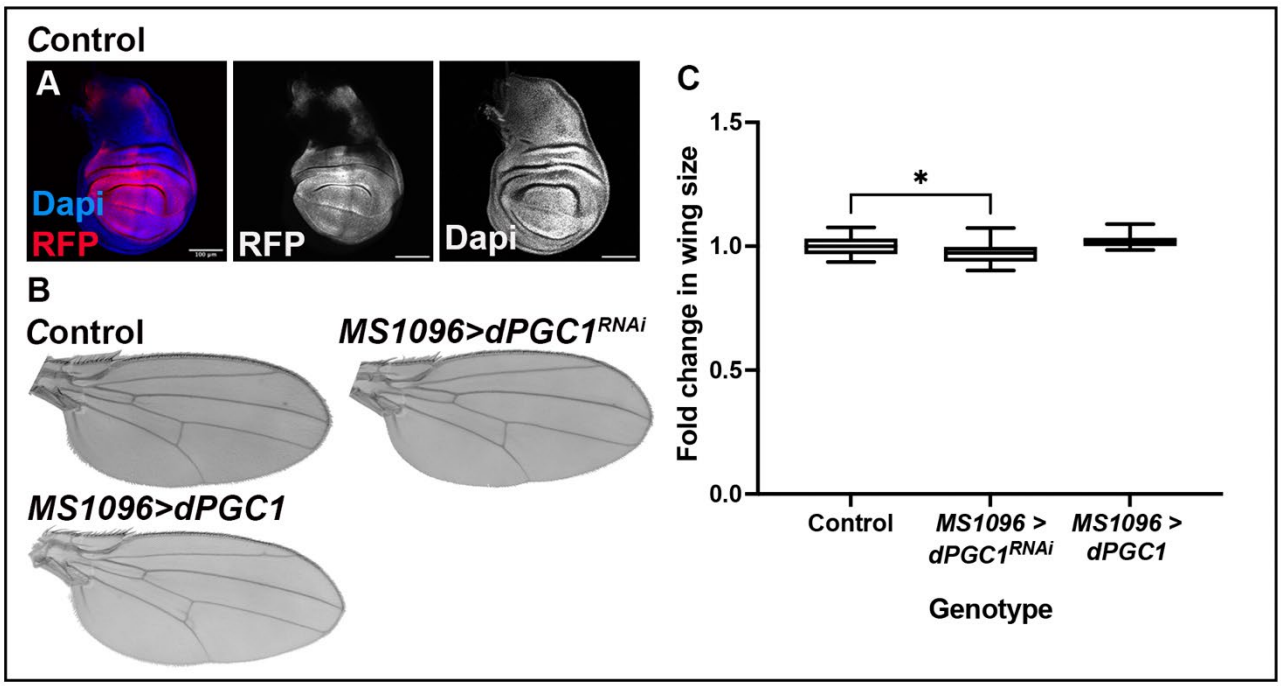

899

900 **Figure 1. dPGC1 in Normal Wing Development.**

901 **(A)** Confocal micrograph showing a *MS1096-Gal4, UAS-RFP* third instar wing imaginal disc. RFP
902 labels the region of the disc expressing this Gal4 line and is shown in red and grey. DAPI labels the
903 DNA and is shown in blue and grey. Scale bar: 100 µm.

904 **(B)** Cuticle preparations of adult wings from *MS1096-Gal4, UAS-lacZ* control flies; *MS1096-Gal4,*
905 *UAS-dPGC1-RNAi* flies*;* and *MS1096-Gal4, EP-dPGC1* flies.

906 **(C)** Quantification of wing size of the genotypes shown in B. Wing area is normalized to the mean of
907 the control. Statistical significance was determined by unpaired t test with Welch's correction (n = 20
908 [MS1096>lacZ], n = 20 [MS1096>dPGC1-RNAi], n = 20 [MS1096>UAS-dPGC1]; *P < 0.05).

909

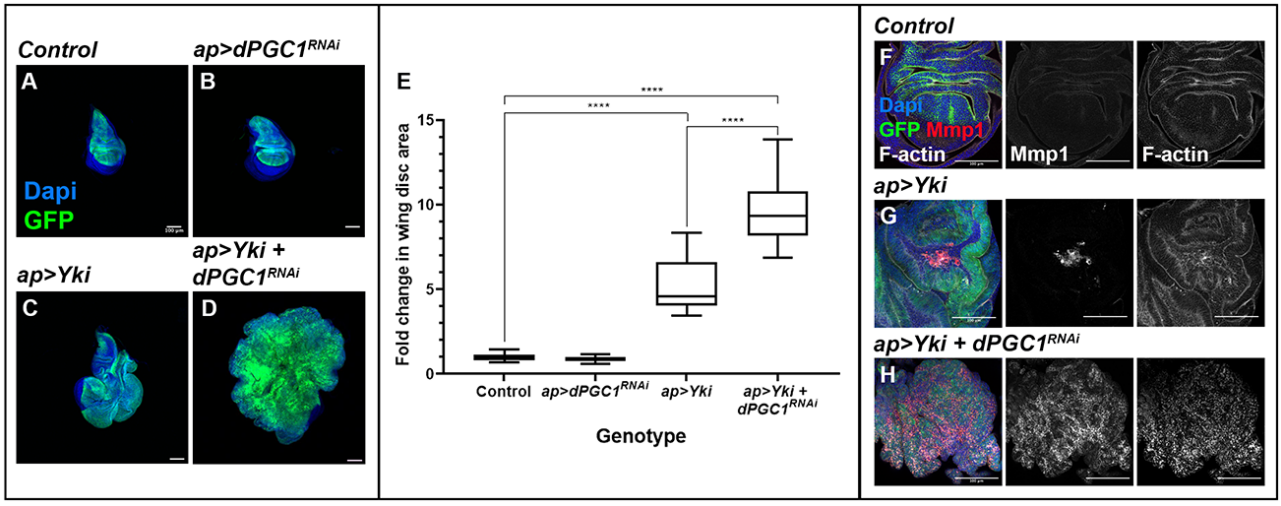

Figure 2. Oncogenic Growth in Discs Over-Expressing Yki and Downregulating dPGC1.

(A-D) Confocal micrographs showing discs of the following genotypes: *ap-Gal4, UAS-GFP, UAS-LacZ* (A); *ap-Gal4, UAS-GFP, UAS-dPGC1-RNAi* (B); *ap-Gal4, UAS-GFP, UAS-Yki, UAS-LacZ* (C); and *ap-Gal4, UAS-GFP, UAS-Yki, UAS-dPGC1-RNAi* (D). GFP is shown in green and DAPI labels the DNA and is shown in blue. Scale bar: 100 μm.

(E) Quantification of GFP-positive area in third-instar wing imaginal discs of the genotypes shown in A-D. GFP-positive area is normalized to the mean of the control. Statistical significance was determined by unpaired t test with Welch's correction (n = 18 [ap>LacZ], n = 19 [ap> dPGC1-RNAi], n = 20 [ap> Yki], n = 20 [ap> Yki, dPGC1-RNAi]; ****P < 0.0001.

(F-H) Confocal micrographs of imaginal discs of the following genotypes: *ap-Gal4, UAS-GFP, UAS-LacZ* (F); *ap-Gal4, UAS-GFP, UAS-Yki, UAS-LacZ* (G); and *ap-Gal4, UAS-GFP, UAS-Yki, UAS-dPGC1-RNAi* (H). F-actin marks cell polarity and is shown in grey. Mmp1 is shown in red and grey. GFP is shown in green. DAPI labels the DNA and is shown in blue. Scale bar: 100 μm. Note the increase in Mmp1 signal and F-actin disorganization in the tumorous disc shown in H, as compared with F and G.

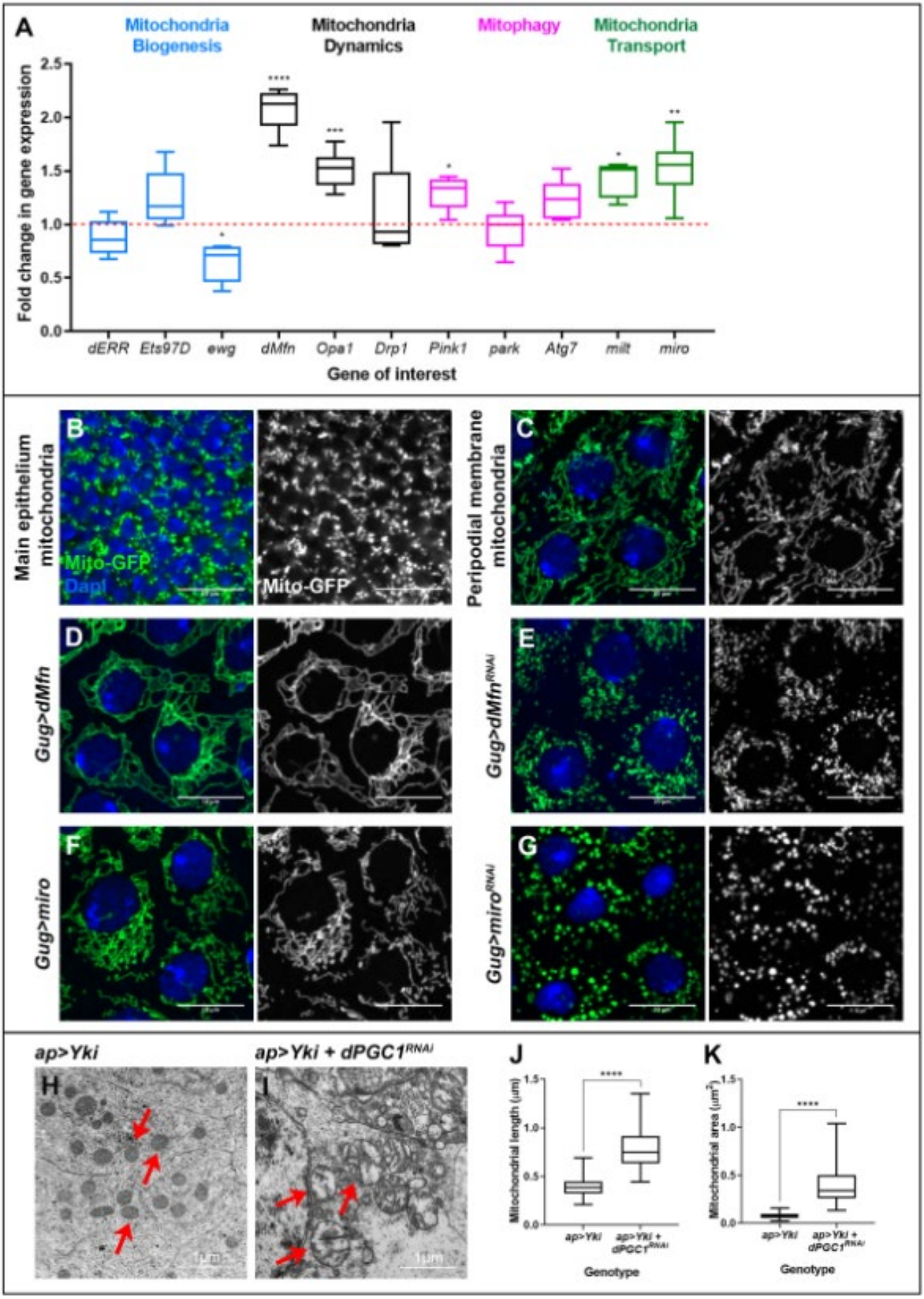
A
Mitochondria Biogenesis
Mitochondria Dynamics
Mitophagy
Mitochondria Transport
Fold change in gene expression
2.5
2.0
1.5
1.0
0.5
0.0
dERR
Ets97D
ewg
dMfn
Opa1
Drp1
Pink1
park
Atg7
milt
miro
Gene of interest
Main epithelium mitochondria
B
Mito-GFP
Dapi
Mito-GFP
Peripodial membrane mitochondria
C
Gug>dMfn
D
Gug>dMfn^RNAi
E
Gug>miro
F
Gug>miro^RNAi
G
ap>Yki
H
ap>Yki + dPGC1^RNAi
I
J
Mitochondrial length (µm)
ap>Yki
ap>Yki + dPGC1^RNAi
Genotype
K
Mitochondrial area (µm²)
ap>Yki
ap>Yki + dPGC1^RNAi
Genotype

926

927 **Figure 3. Aberrant Mitochondrial Dynamics in Yki + dPGC1-RNAi Tumorous Discs.**

928 **(A)** mRNA quantification by qPCR of the genes indicated on the X axis. We separated those genes
929 in different categories: mitochondria biogenesis - blue, mitochondrial dynamics - black, mitophagy -
930 pink, and mitochondrial transport - green. Those genes were quantified in *ap-Gal4, UAS-GFP, UAS-*
931 *Yki, UAS-dPGC1-RNAi*. Control is *ap-Gal4, UAS-GFP, UAS-Yki, UAS-LacZ*. The data show mean
932 ± SD from five to six biological replicates. Data were normalized to RP49. Statistical significance
933 was determined by unpaired t test with Welch's correction for parametric data and by Mann-Whitney
934 test for non-parametric data (*P < 0.05, **P < 0.01, ***P < 0.001, ****P < 0.0001).

935 **(B)** Confocal micrograph of an *ap-Gal4, UAS-mito-GFP* disc showing a XY section of the wing disc
936 main epithelium. Mitochondria are labeled with mito-GFP and are shown in green and grey. DAPI is
937 shown in blue. Scale bar 10 μm.

938 **(C)** Confocal micrograph of a *Gug-Gal4, UAS-mito-GFP, YW* disc showing a XY section of the wing
939 disc peripodial epithelium. Mitochondria are labeled with mito-GFP and are shown in green and grey.
940 DAPI is shown in blue. Scale bar 10 μm.

941 **(D-G)** Confocal micrographs showing XY sections of wing disc peripodial epithelia in the following
942 genotypes: *Gug-Gal4, UAS-mito-GFP, UAS-dMfn* (D); *Gug-Gal4, UAS-mito-GFP, UAS-dMfn-RNAi*
943 (E); *Gug-Gal4, UAS-mito-GFP, UAS-miro* (F); and *Gug-Gal4, UAS-mito-GFP, UAS-miro-RNAi* (G).
944 Mitochondria are labeled with mito-GFP and are shown in green and grey. DAPI is shown in blue.
945 Scale bar 10 μm.

946 **(H, I)** Electron microscopy micrographs obtained from discs of the following genotypes: *ap-Gal4,*
947 *UAS-GFP, UAS-Yki, UAS-LacZ* (H); and *ap-Gal4, UAS-GFP, UAS-Yki, UAS-dPGC1-RNAi* (I). Red
948 arrows point to examples of individual mitochondria. Note the mitochondria size difference between
949 the two conditions analyzed. Scale bar 1 μm.

950 **(J, K)** Quantification of mitochondrial length and mitochondrial area from electron microscopy
951 micrographs obtained from discs of the following genotypes: *ap-Gal4, UAS-GFP, UAS-Yki, UAS-*
952 *LacZ* (control); and *ap-Gal4, UAS-GFP, UAS-Yki, UAS-dPGC1-RNAi* (experimental condition).
953 Statistical significance was determined by unpaired t test with Welch's correction for parametric data
954 and by Mann-Whitney test for non-parametric data (n = 150 [ap> Yki], n = 150 [ap> Yki, dPGC-1-
955 RNAi]; ****P < 0.0001).

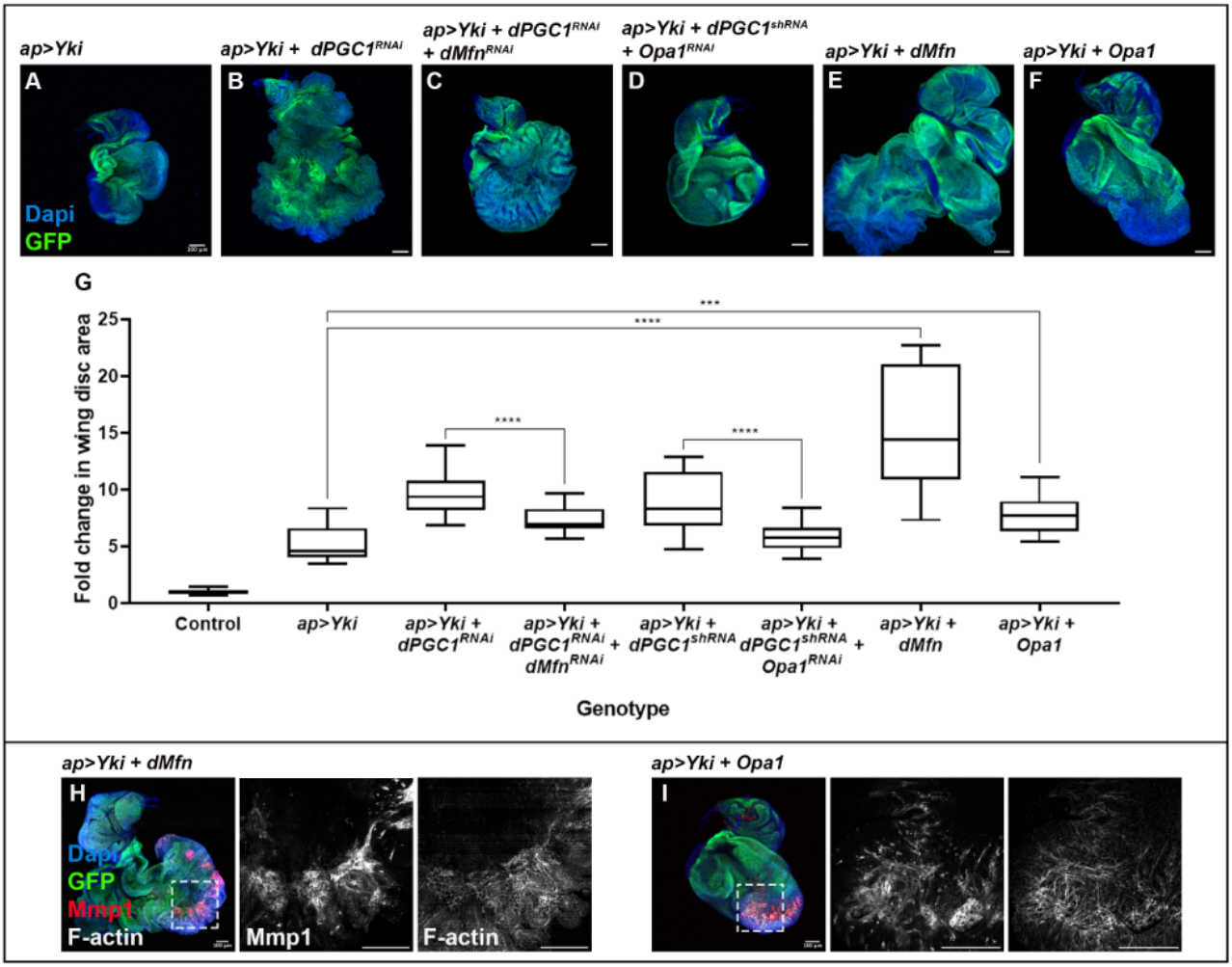

Figure 4. Changes in mitochondrial fusion and fission and tumor formation.

(A-F) Confocal micrographs showing discs of the following genotypes: *ap-Gal4, UAS-GFP, UAS-Yki, UAS-LacZ* (A); *ap-Gal4, UAS-GFP, UAS-Yki, UAS-dPGC1-RNAi* (B); *ap-Gal4, UAS-GFP, UAS-Yki, UAS-dPGC1-RNAi, UAS-dMfn-RNAi* (C); *ap-Gal4, UAS-GFP, UAS-Yki, UAS-dPGC1-shRNA, UAS-Opa1-RNAi* (D); *ap-Gal4, UAS-GFP, UAS-Yki, UAS-dMfn* (E); *ap-Gal4, UAS-GFP, UAS-Yki, UAS-Opa1* (F). GFP is shown in green and DAPI labels the DNA and is shown in blue. Scale bar: 100 μm.

(G) Quantification of GFP-positive area in third-instar wing imaginal discs of the genotypes shown in (A-F). GFP-positive areas are normalized to the mean of the control. Statistical significance was determined by unpaired t test with Welch's correction (n = 18 [ap>LacZ], n = 20 [ap>Yki], n = 20 [ap>Yki, dPGC1-RNAi], n = 20 [ap>Yki, dPGC1-RNAi, UAS-dMfn-RNAi], n = 20 [ap>Yki, dPGC1-shRNA], n = 20 [ap>Yki, dPGC1-shRNA, UAS-Opa1-RNAi], n = 13 [ap>Yki, UAS-dMfn], n = 12 [ap>Yki, UAS-Opa1]; ***P < 0.001, ****P < 0.0001).

(H, I) Confocal micrographs of imaginal discs of the following genotypes: *ap-Gal4, UAS-GFP, UAS-Yki, UAS-dMfn* (H); and *ap-Gal4, UAS-GFP, UAS-Yki, UAS-Opa1* (I). F-actin can be used to visualize cell polarity and epithelial organization, and it is shown in grey. Mmp1 is shown in red and grey. GFP is shown in green. DAPI labels the DNA and is shown in blue. Scale bars: 100 μm.

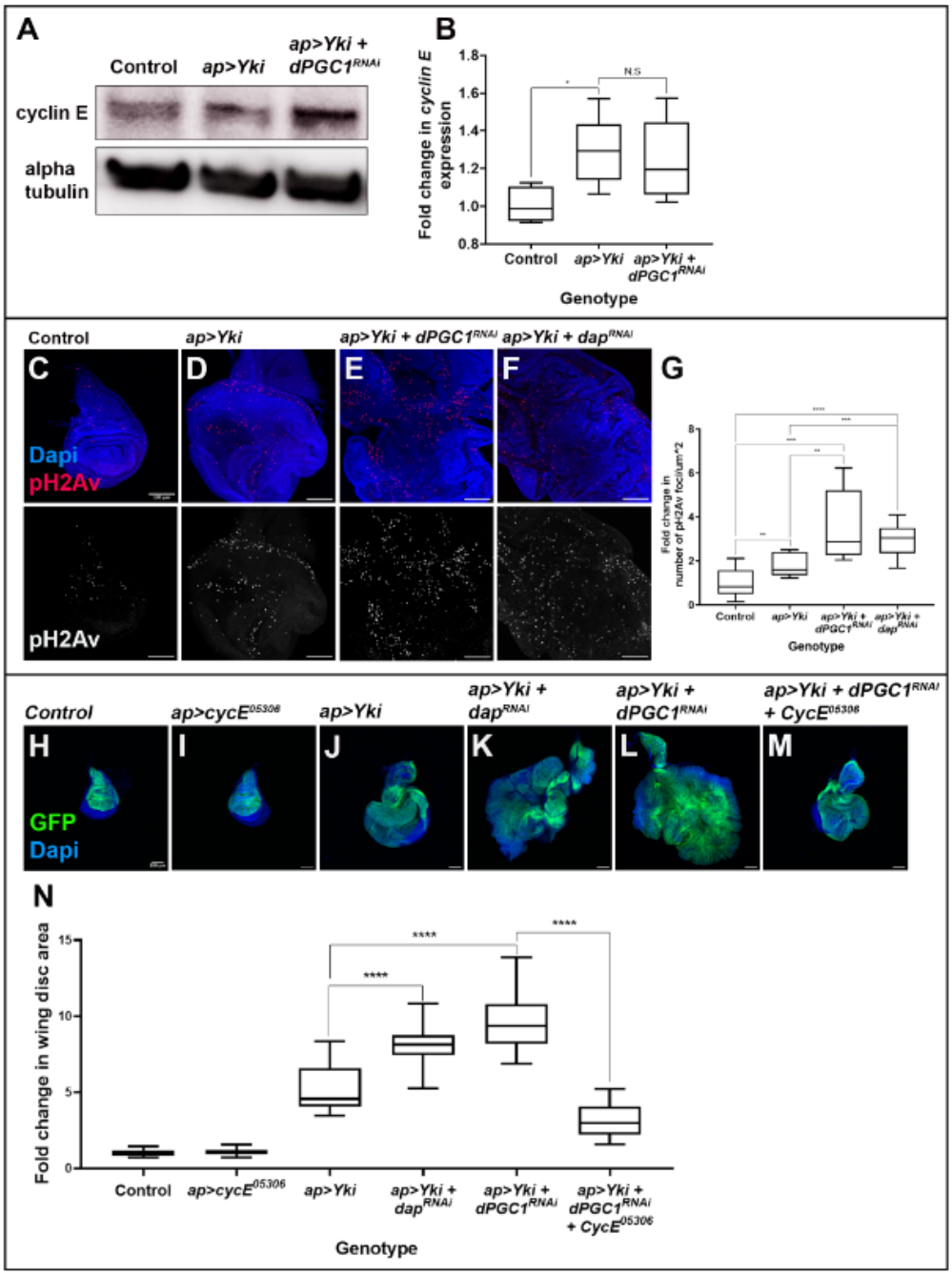

Figure 5. Cyclin E in Yki + dPGC1-RNAi Tumors.

(A) Western blot showing Cyclin E protein in third-instar wing imaginal discs of the genotypes indicated. Alpha-tubulin was used as a loading control.

(B) Quantification of Cyclin E mRNA by qPCR in imaginal discs of the genotypes indicated. The data show mean ± SD for four to five biological replicates. Data were normalized to RP49. Statistical significance was determined by unpaired t test with Welch's (*P < 0.05, N.S indicates not significant).

(C-F) Maximum projection of confocal micrographs of imaginal discs showing phospho-H2Av in red and grey, and DAPI in blue. The genotypes shown are *ap-Gal4, UAS-GFP, UAS-LacZ* (C); *ap-Gal4,*

UAS-GFP, UAS-Yki, UAS-LacZ (D); *ap-Gal4, UAS-GFP, UAS-Yki, UAS-dPGC1-RNAi* (E) and *ap-Gal4, UAS-GFP, UAS-Yki, UAS-dap-RNAi* (F).

(G) Quantification of pH2Av-positive foci in the genotypes shown in C-F. The data were normalized to the mean of the control. Statistical significance was determined by unpaired t test with Welch's correction (n = 12 [ap>LacZ], n = 12 [ap>Yki], n = 12 [ap>Yki, dPGC1-RNAi], n = 20 [ap>Yki, dap-RNAi], ** P<0.01, *** P<0.001, **** P < 0.0001).

(H-M) Confocal micrographs showing discs of the following genotypes: *ap-Gal4, UAS-GFP, UAS-LacZ* (H); *ap-Gal4, UAS-GFP/Cyclin E-05306* (I); *ap-Gal4, UAS-GFP, UAS-Yki, UAS-LacZ* (J); *ap-Gal4, UAS-GFP, UAS-Yki, UAS-dap-RNAi* (K) *ap-Gal4, UAS-GFP, UAS-Yki, UAS-dPGC1-RNAi* (L); *ap-Gal4, UAS-GFP, UAS-Yki, UAS-dPGC1-RNAi/Cyclin E-05306* (M). GFP is shown in green and DAPI labels the DNA and is shown in blue. Scale bar: 100 µm.

(N) Quantification of GFP-positive area in third-instar wing imaginal discs of the genotypes shown in H-M. GFP-positive area is normalized to the mean of the control. Statistical significance was determined by unpaired t test with Welch's correction (n = 18 [ap>LacZ], n = 20 [ap>cyclin E-05306], n = 20 [ap>Yki], n = 20 [ap>Yki, dap-RNAi] n = 20 [ap>Yki, dPGC1-RNAi], n = 20 [ap>Yki, dPGC1-RNAi, cyclin E-05306]; ****P < 0.0001).